bioRxiv preprint doi: https://doi.org/10.1101/2019.12.17.879544; this version posted December 18, 2019. The copyright holder for this preprint (which was not certified by peer review) is the author/funder, who has granted bioRxiv a license to display the preprint in perpetuity. It is made available under aCC-BY-NC-ND 4.0 International license.

Reduced cellular levels of DNA polymerase delta alter replication dynamics and enzymology, and impair lagging-strand processing

Natasha C Koussa[1] and Duncan J. Smith[1,2]

1. Department of Biology, New York University, New York, NY 10003, USA

2. Corresponding author: duncan.smith@nyu.edu

Running title: Global replication defects due to polymerase delta depletion

Keywords: DNA replication, DNA polymerase delta, lagging-strand synthesis, replication origins

Data deposition: Raw and processed sequencing data available on the GEO, accession GSE141884

bioRxiv preprint doi: https://doi.org/10.1101/2019.12.17.879544; this version posted December 18, 2019. The copyright holder for this preprint (which was not certified by peer review) is the author/funder, who has granted bioRxiv a license to display the preprint in perpetuity. It is made available under aCC-BY-NC-ND 4.0 International license.

ABSTRACT

DNA polymerase delta (Pol ∂) plays several essential roles in eukaryotic DNA replication and repair. At the replication fork, Pol ∂ is responsible for the synthesis and processing of the lagging strand; this role requires Pol ∂ to extend Okazaki fragment primers synthesized by Pol α-primase, and to carry out strand-displacement synthesis coupled to nuclease cleavage during Okazaki fragment termination. Destabilizing mutations in human Pol ∂ subunits cause replication stress and syndromic immunodeficiency. Analogously, reduced levels of Pol ∂ in *Saccharomyces cerevisiae* lead to pervasive genome instability. Here, we analyze the how the depletion of Pol ∂ impacts replication initiation and elongation *in vivo* in *S. cerevisiae.* We determine that Pol ∂ depletion leads to a dependence on checkpoint signaling and recombination-mediated repair for cellular viability. By analyzing nascent lagging-strand products, we observe both a genome-wide change in the establishment and progression of replication forks and a global defect in Pol ∂-mediated Okazaki fragment processing. Additionally, we detect significant lagging-strand synthesis by the leading-strand polymerase (Pol ε) in late-replicating regions of the genome when Pol ∂ is depleted. Together, our results are consistent with the presence of least two Pol ∂ complexes in the eukaryotic replisome under normal conditions. We propose that replisomes with sub-stoichiometric Pol ∂ are defective due to competition between nascent lagging-strand primers and terminating Okazaki fragments, and that this competition underlies both the replication and genome stability defects observed when cellular levels of Pol ∂ fall below a critical threshold.

bioRxiv preprint doi: https://doi.org/10.1101/2019.12.17.879544; this version posted December 18, 2019. The copyright holder for this preprint (which was not certified by peer review) is the author/funder, who has granted bioRxiv a license to display the preprint in perpetuity. It is made available under aCC-BY-NC-ND 4.0 International license.

INTRODUCTION

DNA polymerase delta (Pol ∂) is an essential replisome component in all known eukaryotes (1). During lagging-strand synthesis, Pol ∂ extends Okazaki fragment primers synthesized by DNA polymerase alpha/primase (Pol α) (2). Upon reaching the 5' end of the preceding Okazaki fragment, Pol ∂ continues synthesis, iteratively displacing short 5' flap structures that are nucleolytically cleaved by Fen1 and other nucleases (3–5) to replace most or all of the DNA incorporated by the error-prone Pol α (6, 7). Pol ∂ plays an additional role at replication origins, synthesizing a stretch of DNA on the nascent leading strand that is subsequently extended by DNA polymerase epsilon (Pol ε) (8–10). Thus, Pol ∂ is directly responsible for the synthesis of approximately half the nuclear DNA in eukaryotic genomes (11, 12) and is intimately involved in every step of the replication program. Multiple suppression mechanisms exist to maintain the specificity of Pol ε and Pol ∂ for leading- and lagging-strand synthesis, respectively (13, 14). However, Pol ∂ can effectively synthesize the entire leading strand in both budding and fission yeast when the catalytic activity of Pol ε is abrogated (9, 15–17), and recent work suggests that Pol ∂ may take over leading-strand synthesis from Pol ε during replication termination under normal conditions (18).

Mutations affecting the stability or catalytic activity of Pol ∂ are associated with various human diseases. Alleles with reduced replication fidelity, including exonuclease-deficient alleles, are driver mutations for heritable cancers (19–21) and can induce catastrophic genome instability when expressed in yeast (22). A heterozygous active site mutation that abolishes Pol ∂ catalytic activity gives rise to developmental defects including lipodystrophy (23). In addition, mutations that reduce the stability of the Pol ∂ complex have recently been reported as causal for a syndromic immunodeficiency associated with replication stress (24). Some of the phenotypes associated with Pol ∂ deficiency overlap with those reported for Pol ε hypomorphy in a mouse model (25).

bioRxiv preprint doi: https://doi.org/10.1101/2019.12.17.879544; this version posted December 18, 2019. The copyright holder for this preprint (which was not certified by peer review) is the author/funder, who has granted bioRxiv a license to display the preprint in perpetuity. It is made available under aCC-BY-NC-ND 4.0 International license.

The depletion of Pol ∂ in budding yeast via transcriptional repression of the catalytic Pol3 subunit leads to various manifestations of genome instability, including an increase in the frequency of both point mutations and gross chromosomal rearrangements (26–28). However, the underlying basis for these defects could in theory derive from any of the roles of Pol ∂ in DNA replication or repair (29). The DNA replication machinery is highly conserved from yeast to humans. Therefore, directly characterizing the behavior of the yeast replisome under conditions where Pol ∂ is scarce can provide insights into the mechanisms by which Pol ∂ hypomorphs lead to genome instability in multicellular eukaryotes including humans.

Here, we define the short-term effects of both mild and acute Pol ∂ depletion on the DNA replication program in budding yeast via the genome-wide analysis of lagging-strand synthesis, replication-origin firing and DNA polymerase usage. We find that Pol ∂ depletion impairs the firing of early, efficient replication origins, slows replisome movement, and leads to a dependence on checkpoint activation for survival through even a single cell cycle. We further demonstrate that cells with limiting Pol ∂ are defective for Okazaki fragment processing, and provide evidence that Pol ε can participate in lagging-strand synthesis in late-replicating regions of the genome.

bioRxiv preprint doi: https://doi.org/10.1101/2019.12.17.879544; this version posted December 18, 2019. The copyright holder for this preprint (which was not certified by peer review) is the author/funder, who has granted bioRxiv a license to display the preprint in perpetuity. It is made available under aCC-BY-NC-ND 4.0 International license.

RESULTS

In *S. cerevisiae*, Pol ∂ is a heterotrimeric complex (30), comprising the essential Pol3 catalytic subunit and two additional accessory subunits – Pol31 and Pol32. Of the two accessory subunits, only Pol31 is essential for viability as long as the PIP boxes on the other subunits are intact (31). Besides forming part of Pol ∂, Pol31 and Pol32 are integral components of the translesion DNA polymerase ζ (32): we therefore chose to titrate Pol3 to avoid as best as possible any indirect effects due to Pol ζ depletion. Titratable expression of *POL3* from the *GAL1* promoter has previously been used to study the long-term effects of Pol ∂ depletion (26, 27). However, because modulating transcription using galactose is relatively slow and *GAL1-POL3* strains have been reported to revert to high expression with detectable frequency (27), we chose to titrate Pol3 via targeted proteolysis. The resulting rapid degradation of Pol3 was allows us to investigate the immediate consequences of Pol ∂ depletion within a single cell cycle.

In vivo titration of Pol ∂ *in vivo* via controlled proteolysis of Pol3

To rapidly deplete Pol3 from cycling *S. cerevisiae* cells, we tagged the protein with an C-terminal auxin-inducible degron (33) and added a C-terminal 9xMyc tag for detection of Pol3 by western blot. Pol3 depletion in a strain carrying TIR1 (33) was readily detectable after 30 minutes (**Fig. S1A**) and treatment with indoleacetic acid (IAA) at concentrations between 0.01 mM and 1 mM allowed Pol3 levels to be titrated between wild-type and essentially undetectable levels (**Fig. 1A**). Long-term growth in the presence of IAA was impaired as assayed by serial dilution of cells on solid media (**Fig. 1B**) and cell density in liquid media (**Fig. S1B**). Cells were viable even at 1 mM IAA (**Fig. 1B, S1B**). Analysis of DNA content by flow cytometry in synchronized cultures indicated that low Pol3 levels delayed both entry into S-phase and extended its duration (**Fig. 1C**). Consistent with these data, asynchronous cultures treated with high concentrations of IAA accumulated in G1 and S-phase (**Fig. S1C**).

bioRxiv preprint doi: https://doi.org/10.1101/2019.12.17.879544; this version posted December 18, 2019. The copyright holder for this preprint (which was not certified by peer review) is the author/funder, who has granted bioRxiv a license to display the preprint in perpetuity. It is made available under aCC-BY-NC-ND 4.0 International license.

Conditional depletion of Pol ∂ leads to checkpoint activation, DNA damage, and dependence on recombination-mediated repair

We assayed checkpoint activation during Pol3 depletion by western blot against Rad53 following 2h of treatment with increasing concentrations of IAA (**Fig. 2A**). Phosphorylation of Rad53 was apparent from 0.2 mM IAA – the lowest concentration that leads to a growth defect in *POL3-AID* strains (**Fig. 1B**). Rad53 phosphorylation can occur via the DNA replication checkpoint (DRC), dependent on Mrc1, or the DNA damage checkpoint (DDC), mediated by Rad9 (34). We tested Rad53 phosphorylation in *POL3-AID* strains deleted for either *MRC1* or *RAD9*, or for the apical kinase *MEC1*, which is required for both pathways (**Fig. 2A**). As expected, Rad53 phosphorylation was virtually abolished in a *mec1Δ;sml1Δ* strain. Deletion of *RAD9* substantially reduced the extent of Rad53 phosphorylation, especially at lower concentrations of IAA, while deletion of *MRC1* had a much weaker effect, (**Fig. 2A**). We therefore conclude that Pol ∂ scarcity leads to checkpoint activation, predominantly through the DDC but with a contribution from the DRC.

We next tested whether checkpoint activation was required to maintain the viability of *POL3-AID* cells during Pol3 depletion. Both *POL3-AID;mec1Δ;sml1Δ* and *POL3-AID;rad53Δ;sml1Δ* strains showed severe growth phenotypes even at 0.05 mM IAA (**Fig. 2B**), when Pol3 concentrations are only slightly reduced (**Fig. 1A**). Furthermore, consistent with the relative contributions of the DDC and DRC to Rad53 phosphorylation (**Fig. 2A**), the *POL3-AID;rad9Δ* strain had a stronger growth defect than *POL3-AID;mrc1Δ* at moderate concentrations of IAA (**Fig. 2B**). Depletion of Pol3 for 2-4h was sufficient to cause widespread cell death in the *mec1Δ;sml1Δ* background, as assayed by serial dilution spot tests of cells allowed to recover on YPD plates after transient treatment with 1 mM IAA (**Fig. 2C**). Under these conditions, G1-arrested *mec1Δ;sml1Δ* cells depleted for Pol3 were able to enter S-phase, but few if any cells reached G2 100 minutes after release from G1 (**Fig. 2D**).

bioRxiv preprint doi: https://doi.org/10.1101/2019.12.17.879544; this version posted December 18, 2019. The copyright holder for this preprint (which was not certified by peer review) is the author/funder, who has granted bioRxiv a license to display the preprint in perpetuity. It is made available under aCC-BY-NC-ND 4.0 International license.

The requirement for checkpoint activation, particularly via the DDC, suggested that DNA damage may accumulate during Pol3 depletion. We tested for the accumulation of DNA double-strand breaks (DSBs) via western blots against histone H2A phosphorylated at Serine 129 (phosphor-H2A) following 2h of IAA treatment (**Fig. 2E**). Phospho-H2A was detectable at IAA concentrations over 0.05 mM – the same concentration at which *mec1Δ;sml1Δ* cells begin to show an obvious growth phenotype (**Fig. 2C**). To test which pathway is required for the repair of DSBs caused by Pol3 depletion, we deleted the homologous recombination (HR) factors *RAD51*, *RAD52* or *MRE11*, as well as the non-homologous end-joining factor *YKU70*. Deletion of *RAD51, RAD52* or *MRE11* substantially decreased viability at moderate IAA concentrations; by contrast, abrogation of end-joining via deletion of *YKU70* slightly increased fitness under these conditions (**Fig. 2F**). This indicates that DSBs occurring due to Pol3 depletion are repaired by HR-mediated mechanisms.

Homologous recombination is largely restricted to late S and G2, while DNA damage arising as a result of Pol ∂ scarcity is likely to occur throughout both early- and late-replicating regions of the genome. The accumulation of single-stranded DNA in those regions could further contribute to checkpoint activation. To explore the possibility that single-stranded DNA is more abundant when Pol ∂ is scarce, and that gaps persist through S-phase in Pol3 depletion, we assayed the level of RPA bound to chromatin via western blot against Rfa1 following subcellular fractionation (**Fig. 2G**). After 2h of IAA treatment, both the total and chromatin-bound pools of RPA increased substantially. To exclude the possibility that this increase simply reflected the accumulation of IAA-treated cells in S-phase (**Fig. S1C**), we assayed Rfa1 levels after synchronous release into S-phase (**Fig. 2H**). Chromatin-bound RPA was highly enriched in both mid and late S-phase in IAA-treated cells compared to untreated controls, implying the persistence of single-stranded DNA throughout S-phase.

Together, these data suggest that depletion of Pol3, and consequently Pol ∂, rapidly leads to the accumulation of single-stranded DNA and double-strand breaks, leading to checkpoint activation and

bioRxiv preprint doi: https://doi.org/10.1101/2019.12.17.879544; this version posted December 18, 2019. The copyright holder for this preprint (which was not certified by peer review) is the author/funder, who has granted bioRxiv a license to display the preprint in perpetuity. It is made available under aCC-BY-NC-ND 4.0 International license.

delayed progression through S-phase. HR-mediated DNA repair pathways are essential for cells with limiting Pol ∂ to complete S-phase and continue through the cell cycle.

Effects of limiting Pol ∂ on productive replication origin firing *in vivo*

Pol ∂ is responsible for the majority of DNA replication on the lagging strand (11, 12), but also plays a key role in the initiation of leading-strand synthesis at replication origins (8–10). To investigate the effect of Pol3 depletion on origin firing, we sequenced Okazaki fragments from asynchronous strains depleted for Pol3. We compared the effects of progressively lower Pol ∂ levels for two biological replicate strains grown in YPD alone or supplemented with 0.2 mM, 0.6 mM, or 1 mM IAA. Data showing the average behavior of two replicates are shown in **Fig. 3**, and individual replicates are shown separately in **Fig. S2**. Cultures were treated with IAA for 2h before the addition of rapamycin for 1h to deplete DNA ligase I (Cdc9) from the nucleus via anchor-away (35). As previously described (36), we quantified origin firing efficiency as the Origin Efficiency Metric (OEM), based on the fraction of Okazaki fragments mapping to either the Watson or Crick strand in a window ±10 kb around previously validated replication origins: OEM represents the fraction of cells in the population in which a given origin fires.

Analysis of Okazaki fragment strand bias across the genome suggested that the average direction of replication was relatively similar at most loci across all Pol3 depletion conditions (**Fig. 3A**). Surprisingly, quantitative analysis of origin firing (**Fig. 3B**) revealed a statistically significant increase in the average firing efficiency – expressed as OEM – upon Pol3 depletion ($p = 0.0205$ for 0 mM vs 1 mM by Wilcoxon signed rank test), accompanied by a change in the distribution of these efficiencies ($p < 0.0001$ for 0 mM vs 1 mM by Kolmogorov-Smirnov test). Direct comparison of firing efficiencies in YPD compared to YPD + 1 mM IAA indicated that Pol3 depletion slightly decreased the firing efficiency of the most efficient origins, while increasing the efficiency of normally weak origins (**Fig. 3C**). Because origin firing efficiency in *S. cerevisiae* correlates strongly with replication timing, we

bioRxiv preprint doi: https://doi.org/10.1101/2019.12.17.879544; this version posted December 18, 2019. The copyright holder for this preprint (which was not certified by peer review) is the author/funder, who has granted bioRxiv a license to display the preprint in perpetuity. It is made available under aCC-BY-NC-ND 4.0 International license.

reasoned that the increased firing of inefficient origins could be related to their late replication. We assigned origins as early or late based on their median replication time (T_{rep}) in a previous study (37), and separately analyzed the change in efficiency for early- and late-firing origins (**Fig. 3D-E**). Consistent with a strong effect of firing time, we observed a significant increase in the firing efficiency of late origins during Pol3 depletion (**Fig. 3E**. $p < 0.0001$ for 0 mM vs 1 mM by Wilcoxon signed rank test), accompanied by a decrease in early origin firing (**Fig. 3D**. $p < 0.0001$ for 0 mM vs 1 mM).

Replication-fork speed is reduced when Pol ∂ is limiting

The progressive increase in firing efficiency of late-replicating origins at lower Pol3 concentrations (**Fig. 3E**) could be at least partly explained by decreased replication-fork mobility, which would reduce passive replication of these origins and instead allow them to fire. To test this, we sequenced Okazaki fragments from strains synchronously released into S-phase at 25 ˚C in YPD ±1 mM IAA (flow cytometry data showing the timepoints selected for analysis are in **Fig. S3**). Okazaki fragment sequencing data from this time course are shown in **Fig. 4A**. The density of sequencing reads in cultures sampled from 45-60 minutes after release showed decreased replication of origin-distal regions upon Pol3 depletion (**Fig. 4A**), consistent with delayed origin firing and/or reduced fork speed.

To confirm that Pol3 depletion globally decreases replisome mobility, we carried out meta-analysis of both total (**Fig. 4B**) and strand-specific (**Fig. 4C**) Okazaki fragment density 20 kb up- and downstream of early-firing origins. Total Okazaki fragment density monitors the extent to which the lagging strand has been replicated, regardless of the direction of fork movement. By contrast, the stranded analysis considers only Okazaki fragments from leftward-moving forks to the left of the origin, and from rightward-moving forks to the right – these data therefore report more directly on the movement of forks emanating from the origins being analyzed. In both cases, Okazaki fragments from Pol3-depleted cells generated a sharper peak close to early-firing origins after 45 minutes, which propagated away from origins more slowly than for cells grown in YPD (**Fig. 4B, 4C**). We therefore

bioRxiv preprint doi: https://doi.org/10.1101/2019.12.17.879544; this version posted December 18, 2019. The copyright holder for this preprint (which was not certified by peer review) is the author/funder, who has granted bioRxiv a license to display the preprint in perpetuity. It is made available under aCC-BY-NC-ND 4.0 International license.

conclude that the progression of replication forks through the genome is impaired when Pol ∂ is limiting. However, we note that our data do not distinguish between the global slowing of all forks and normal fork speed punctuated by widespread fork stalling.

Taken together, the global changes in replication-origin firing efficiency and replication-fork progression are most consistent with a model whereby severely limiting Pol ∂ globally impairs origin firing *in vivo*, albeit surprisingly mildly. Because fork progression is impeded when Pol ∂ is scarce, normally late-firing origins are less likely to be passively replicated and the net effect is an increase in their firing efficiency. An analogous global decrease in replication-origin firing efficiency has been observed in Pol ∂-deficient human fibroblasts (24).

Pol ∂ depletion alters lagging-strand biogenesis without affecting Okazaki fragment size

Given Pol ∂'s role as the major lagging-strand polymerase, we anticipated that one or more steps required for Okazaki fragment biogenesis – i.e. initiation, synthesis, and processing – could be impacted by depletion of Pol3. We first assayed the length of end-labeled Okazaki fragments obtained after Cdc9 anchor away during Pol3 depletion in asynchronous cultures. Surprisingly, we observed a that the overall length distribution of Okazaki fragments was unchanged, but the normal nucleosome-based phasing of fragment size (7) was lost at IAA concentrations greater than 0.1 mM (a representative gel is shown in **Fig. 5A**, and a replicate in **Fig. S4A**). We additionally verified this result in a strain carrying an AID-tagged version of the Pol31 protein. When Pol31 was depleted, nucleosome-based phasing of Okazaki fragment size was again absent at IAA concentrations above 0.1 mM (**Fig. S4B**).

We have previously observed a loss of nucleosome-based Okazaki fragment phasing in strains deficient for Okazaki fragment processing, including a Rad27 conditional depletion strain. When lagging-strand processing by nick translation is impaired by the absence of Rad27, Okazaki fragment

bioRxiv preprint doi: https://doi.org/10.1101/2019.12.17.879544; this version posted December 18, 2019. The copyright holder for this preprint (which was not certified by peer review) is the author/funder, who has granted bioRxiv a license to display the preprint in perpetuity. It is made available under aCC-BY-NC-ND 4.0 International license.

termini are enriched on the replication-fork proximal sides of nucleosome dyads (38). We confirmed that this phenotype occurs in our *POL3-AID* strain. Increasing concentrations of IAA shifted the peak of Okazaki fragment 5' and 3' termini progressively upstream of the nucleosome dyad (**Fig. 5B & replicate data in Fig. S4C**), as previously observed for Okazaki fragment processing mutants (38). To further confirm the decreased nick translation during Pol3 depletion outside nucleosomes, we aligned Okazaki fragment termini around Abf1, Reb1 and Rap1 binding sites; these general regulatory factors present 'hard' barriers to strand-displacement synthesis by Pol ∂, leading to a sharp peak of Okazaki fragment termini (7) that is reduced when nick translation is impaired (38). Consistent with the other phenotypes described above, Okazaki fragment termini were progressively less enriched at Abf1/Reb1/Rap1 sites as Pol3 was increasingly depleted (**Fig. 5C** and replicate data in **Fig. S4D**). Taken together, our data are consistent with Pol3 depletion leading to a global defect in lagging-strand processing via a reduction in nick translation by Pol ∂.

Pol ε contributes to lagging-strand synthesis in late-replicating regions when Pol ∂ is limiting

The defects observed in nick translation and Okazaki fragment processing during Pol3 depletion suggested at least two possibilities that are not mutually exclusive. In the context of limiting Pol ∂, the polymerase might prematurely disengage from the terminating Okazaki fragment as opposed to remaining associated for iterative rounds of strand-displacement synthesis. Alternatively, one or more alternative polymerases may be contributing to bulk lagging-strand synthesis under these conditions. Extensive use of an alternative polymerase is expected to impair nick translation because Pol ∂ has a much higher strand-displacement synthesis activity than other DNA polymerases in yeast (39). Synthesis by Pol α is inhibited by RFC-dependent loading of PCNA (15, 40), but Pol ε has been reported to compete weakly with Pol ∂ for lagging-strand primers *in vitro* (13). In addition, any of the three translesion polymerases present in *S. cerevisiae* could contribute: indeed, Pol η has recently been reported to participate in lagging-strand synthesis to a measurable extent (41).

bioRxiv preprint doi: https://doi.org/10.1101/2019.12.17.879544; this version posted December 18, 2019. The copyright holder for this preprint (which was not certified by peer review) is the author/funder, who has granted bioRxiv a license to display the preprint in perpetuity. It is made available under aCC-BY-NC-ND 4.0 International license.

To test the possibility that translesion (TLS) DNA polymerases might contribute substantially to DNA replication during Pol3 depletion, we combined the *POL3-AID* allele with individual knockouts of *REV1, REV3* and *RAD30* (Pol η), as well as the *rev1;rev3;rad30* triple mutant (*ΔTLS*). Individual or simultaneous deletion of the three TLS polymerases failed to exacerbate the growth phenotype observed during Pol3 depletion at any concentration of IAA (**Fig. 6A**). We conclude that growth during transient Pol ∂ depletion is not rescued by the widespread action of TLS polymerases.

In order to investigate the overall contribution of Pol ε to DNA replication in the context of Pol ∂ depletion, we combined *POL3-AID* with the *pol2-M644G* allele of the catalytic subunit of Pol ε: this allele causes increased incorporation of ribonucleotides into the nascent leading strand (42). In strains unable to remove single ribonucleotides from genomic DNA due to deletion of the RNase H2 subunit *RNH202*, ribonucleotide positions can be tracked by HydEn-seq. Ribonucleotides are cleaved by alkaline hydrolysis, followed by strand-specific high-throughput sequencing to identify their locations (11). Ribonucleotides incorporated by Pol ε are normally highly specific for the leading strand, so an increased contribution of Pol ε to lagging-strand synthesis during Pol ∂ depletion should result in a loss of strand bias for Pol ε-derived ribonucleotides (**Fig. 6B**).

We prepared HydEn-seq libraries from two biological replicate *POL3-AID;pol2-M644G;rnh202Δ* strains grown ± 1 mM IAA for 2h before genomic DNA preparation. Average results for the two strains at 0 mM and 1 mM IAA are shown in **Fig. 6**, and results for individual replicates in **Fig. S5**. We observed a subtle reduction in the strand bias of ribonucleotide incorporation by Pol ε within the region 10 kb up- and downstream of replication origins when Pol3 was depleted at 1 mM IAA (**Fig. 6C**).

bioRxiv preprint doi: https://doi.org/10.1101/2019.12.17.879544; this version posted December 18, 2019. The copyright holder for this preprint (which was not certified by peer review) is the author/funder, who has granted bioRxiv a license to display the preprint in perpetuity. It is made available under aCC-BY-NC-ND 4.0 International license.

Pol3 depletion has opposing effects on the firing efficiencies of early- and late-firing replication origins (**Fig. 3E-F**), which means that the same strand cannot necessarily be assigned as lagging at different auxin concentrations. Moreover, the stable association of scarce Pol ∂ complexes with elongating replisomes emanating from early-firing origins might cause replisomes assembling later in S-phase to be differentially sensitive to Pol3 depletion. We therefore separately analyzed ribonucleotide incorporation by Pol ε around early and late origins, taking into account the change in lagging-strand bias inferred from the Okazaki fragment sequencing experiments shown in **Fig. 3**.

Around early-firing origins – defined as origins with a T_{rep} below the median for the 281 origins analyzed (37) – the increase in ribonucleotide density on the predicted lagging strand corresponded precisely to the change in lagging-strand identity arising from the reduced firing of these origins (**Fig. 6D**). Therefore, we conclude that during Pol ∂ depletion the ribonucleotide distribution in early replicating regions changed purely as a result of altered origin firing (as opposed to changes in the enzymology of the resulting replisomes). In contrast, we observed strikingly different results around late-firing origins (**Fig. 6E**). If strict segregation of Pol ε to the leading strand were maintained, the increased firing efficiency of these origins would result in increased ribonucleotide incorporation on the Crick strand to the left of origins, with a corresponding decrease to the right. By contrast, the change in ribonucleotide distribution had the opposite polarity to the change in average replication-fork direction (**Fig. 6E**). Therefore, although the polarization of lagging-strand identity around late origins is increased by Pol3 depletion, there is a substantial reduction in the strand bias of ribonucleotide incorporation by Pol ε that more than offsets the change in average replication direction. We therefore conclude that the discrimination of Pol ε for the leading strand is reduced in late-replicating regions of the genome when Pol ∂ is scarce, resulting in a detectable contribution of Pol ε to lagging-strand synthesis.

By subtracting the change in replication-fork polarity from the change in ribonucleotide incorporation, we estimated the contribution of Pol ε to lagging-strand synthesis in early- and late-replicating regions

bioRxiv preprint doi: https://doi.org/10.1101/2019.12.17.879544; this version posted December 18, 2019. The copyright holder for this preprint (which was not certified by peer review) is the author/funder, who has granted bioRxiv a license to display the preprint in perpetuity. It is made available under aCC-BY-NC-ND 4.0 International license.

(**Fig. 6F**). We observe a ~10% reduction in strand discrimination around late origins. Because complete synthesis of the lagging strand by Pol ε would lead to a 50% reduction in bias over many cell cycles (**Fig. 3B**) but only at most half of the DNA in the culture is nascent after 2h of IAA treatment, the maximum theoretical increase in Pol ε contribution under these conditions is 25%. We therefore propose that Pol ε is either synthesizing all of the lagging strand at a subset of replication forks, or a fraction of the lagging strand at most forks established in late S-phase. Our data cannot formally rule out the alternative scenario, not mutually exclusive with Pol ε replication on the lagging strand, whereby RNA primers are retained in the genome during Pol ∂ depletion. However, because nick translation appears to be similarly impaired in early- and late-replicating regions (**Fig. S6**) while ribonucleotide strand bias changes exclusively in late-replicating regions (**Fig. 6E-F**), we favor the interpretation that invokes Pol ε synthesis on the lagging strand.

bioRxiv preprint doi: https://doi.org/10.1101/2019.12.17.879544; this version posted December 18, 2019. The copyright holder for this preprint (which was not certified by peer review) is the author/funder, who has granted bioRxiv a license to display the preprint in perpetuity. It is made available under aCC-BY-NC-ND 4.0 International license.

DISCUSSION

By directly analyzing the products of lagging-strand synthesis following proteolytic titration of Pol3 in *S. cerevisiae*, we identified several immediate consequences of Pol ∂ depletion for DNA replication. Extremely low levels of Pol ∂ support viability if the checkpoint and recombination-mediated repair pathways are intact (**Fig. 2**). However, replication origin firing (**Fig. 3**), the progression of the resulting replication forks through the genome (**Fig. 4**), and lagging-strand processing (**Fig. 5**) are all progressively impaired as the concentration of Pol ∂ is reduced. In addition, we show that the enzymology of DNA replication is altered in late-replicating regions of the genome when Pol ∂ is scarce, such that Pol ε now contributes detectably to lagging-strand synthesis (**Fig. 6**).

Pol ∂ is required for normal replication origin firing, and synthesizes both the leading and lagging strands in the immediate vicinity of origins *in vivo* (9), consistent with *in vitro* data demonstrating that leading-strand synthesis can proceed via extension of the first Okazaki fragment on the lagging strand (8). The reduction in origin firing efficiency that we observe for early origins (**Fig. 3**) is surprisingly modest given this essential role, although the delayed entry into S-phase observed under these conditions is likely caused by slow recruitment of scarce Pol ∂. Although Pol ∂ deficiency reduces the disparity in firing efficiencies between replication origins compared to unperturbed conditions (**Fig. 3**), the overall replication timing program appears to be largely conserved (**Fig. 4**). Even if Pol ∂ recruitment becomes limiting for origin firing, this binding is still more favorable for early-firing origins. Estimates of Pol3 and Pol31 protein levels in *S. cerevisiae* vary substantially (43). The observation that our strain completes S-phase with no discernible delay at 0.2 mM IAA (**Fig. 1C**) – a concentration that reduces Pol3 levels at least tenfold (**Fig. 1A**) – implies that the normal cellular levels of Pol ∂ are greatly in excess of the minimal amounts needed for timely replication of the genome during rapid growth. However, checkpoint activation is required for survival after even a mild reduction in Pol3 levels (**Fig. 2**), suggesting that at least a proportion of forks encounter difficulties under these conditions.

bioRxiv preprint doi: https://doi.org/10.1101/2019.12.17.879544; this version posted December 18, 2019. The copyright holder for this preprint (which was not certified by peer review) is the author/funder, who has granted bioRxiv a license to display the preprint in perpetuity. It is made available under aCC-BY-NC-ND 4.0 International license.

Elongating replication forks in cells severely depleted for Pol ∂ have at least two obvious defects: they progress slowly (**Fig. 4**) and are impaired for normal Okazaki fragment maturation (**Fig. 5**). Extension of Okazaki fragments by Pol ε would decrease nick translation because Pol ε is deficient for strand-displacement synthesis (15, 39). But the changes in nick translation that we observe are global (**Fig. 5A, S4A-B, S6**), and are therefore unlikely to arise exclusively from lagging-strand synthesis by Pol ε since this only occurs at detectable levels in late-replicating regions (**Fig. 6**). Therefore, impaired fork progression and lagging-strand processing during Pol3 depletion must be reconciled with recently reported data *in vitro* (44) and *in vivo* (45) showing that Pol ∂ remains stably associated with replication forks for long periods of time while undergoing concentration-dependent exchange (44). How could depletion of such a stably associated Pol ∂ complex give rise to the phenotypes we observe?

Pol ∂ has two somewhat distinct roles during lagging-strand synthesis. It extends PCNA-bound primer-template junctions resulting from Pol α/primase synthesis (2), and also engages at nicks generated by iterative rounds of Pol ∂ strand-displacement synthesis followed by Fen1 cleavage during Okazaki fragment processing (5). Assuming that Okazaki fragment priming often occurs before processing of the prior fragment is completed, two competing Pol ∂ substrates repeatedly coexist within the same replisome. Thus, a single stably associated Pol ∂ complex must effectively 'choose' between the nick translation and elongation reactions. Delayed extension of Pol α products would lead to an accumulation of single-stranded DNA and primer template junctions, likely leading to both checkpoint activation and to slower fork movement. Conversely, premature dissociation from the Okazaki fragment terminus to extend the subsequent fragment would lead to an overall reduction in nick translation. We observe all three of the above phenotypes (fork slowing, checkpoint activation, and impaired nick translation). We therefore propose that one stably associated Pol ∂ complex is minimally required per replisome, but that two Pol ∂ are necessary for optimal synthesis by the *S. cerevisiae* replisome *in vivo* (**Fig. 7**). According to this model, the increasingly severe defects we

bioRxiv preprint doi: https://doi.org/10.1101/2019.12.17.879544; this version posted December 18, 2019. The copyright holder for this preprint (which was not certified by peer review) is the author/funder, who has granted bioRxiv a license to display the preprint in perpetuity. It is made available under aCC-BY-NC-ND 4.0 International license.

observe as Pol3 levels are reduced reflect an increasing number of replisomes with only one Pol ∂. Single-molecule studies have shown a single Pol ∂ present in a reconstituted replisome assembled on a forked DNA substrate (44) – an observation that initially appears to be in conflict with our model. It is possible that additional factors that stimulate Pol ∂ recruitment are present *in vivo*, or indeed that physically coupled sister replisomes (46) may share multiple Pol ∂ complexes as recently proposed for Pol α (47). Our model speculates that replisomes with one Pol ∂ can complete replication, albeit with defects in fork progression and Okazaki fragment maturation. Furthermore, lagging-strand processing has not been directly investigated in the reconstituted replisomes shown to contain a single Pol ∂ (44). We therefore do not believe that our data contradict previous reports.

Assuming stable binding of Pol ∂ to the replisome, the concentration of free Pol ∂ will be further reduced in late S-phase by sequestration of the few available complexes in slowly progressing replisomes. Under these conditions, the suppression mechanisms that restrain Pol ε from lagging-strand synthesis (13) are apparently overcome; Pol ε therefore extends lagging-strand primers in a fraction of replisomes assembled at late-firing origins (Fig. 6). In theory, these replisomes could represent either complexes from which Pol ∂ has dissociated, or complexes that never recruited Pol ∂. Our data cannot distinguish between these possibilities.

Low levels of Pol ∂ in *S. cerevisiae* increase both point mutation frequency (26) and large-scale genomic rearrangements (27). In human fibroblasts, hypomorphic Pol ∂ results in the accumulation of Rad51 and 53BP1 foci in addition to altering replication dynamics (24). Our data suggest distinct underlying mechanisms for these phenotypes (**Fig. 7**). Depleting Pol ∂ reduces nick translation (**Fig. 5**). Elevated mutagenesis has previously been observed in *S. cerevisiae* mutants that impair nick translation during lagging-strand synthesis (48, 49), commensurate with the extent to which nick translation is perturbed (38) and presumably due to increased retention of Pol α-derived DNA in the daughter genome. Our model also invokes an increased lifetime for single-stranded DNA on the

bioRxiv preprint doi: https://doi.org/10.1101/2019.12.17.879544; this version posted December 18, 2019. The copyright holder for this preprint (which was not certified by peer review) is the author/funder, who has granted bioRxiv a license to display the preprint in perpetuity. It is made available under aCC-BY-NC-ND 4.0 International license.

lagging-strand template, which would increase both the frequency of one-ended double-strand breaks at replication forks and the sensitivity of Pol ∂-deficient cells to DNA damaging agents that preferentially target single-stranded DNA. Finally, the persistent chromatin-bound RPA observed through S-phase (**Fig 2H**) is consistent with the presence of potentially recombinogenic single-stranded gaps. In human cells, such gaps would be substrates for post-replicative repair mediated by 53BP1 and Rad52(50). Thus, the distinct effects of Pol ∂ scarcity on lagging-strand primer extension and Okazaki fragment processing can each contribute to genome instability via related but independent mechanisms.

bioRxiv preprint doi: https://doi.org/10.1101/2019.12.17.879544; this version posted December 18, 2019. The copyright holder for this preprint (which was not certified by peer review) is the author/funder, who has granted bioRxiv a license to display the preprint in perpetuity. It is made available under aCC-BY-NC-ND 4.0 International license.

MATERIALS AND METHODS

Yeast strains

All strains are W303 RAD5+ background and contained additional mutations required for anchor-away depletion of Cdc9. The genotype of the wild-type strain is *tor1-1::HIS3, fpr1::NatMX4, RPL13A-2xFKBP12::TRP1, CDC9-FRB::HygMX*. The Pol3 depletion strain contains OsTIR1 integrated at the *URA3* locus and *POL3* tagged with IAA17(71-116)-9xmyc (Addgene #99522) as described in (51). Individual knockout strains were created by gene replacement. Ribonucleotide-hyperincorporating strains were a generous gift from Hannah Klein. All mutations were introduced into the *POL3-AID* background by cross, except for *rad52*. Biological replicate strains represent independent colonies derived from one or more crosses.

Cell growth, spot tests, and cell-cycle synchronization

Yeast were grown in YPD at 30C unless indicated otherwise. 3-indoleacetic acid (IAA) (Sigma I2886-5G) was dissolved in 95% ethanol to 200mM. For short term experiments, IAA was added to log phase cells for two hours, followed by addition of 1ug/mL rapamycin (Spectrum 41810000-2) for one hour for Okazaki fragment analysis. Spot tests were performed with exponentially growing cultures (OD 0.65), washed in sterile water, and diluted five-fold in sterile water in 96-well plates and spotted on plates at 30C for two days. For synchronized S-phase analysis, log phase cells (OD 0.2) were briefly sonicated to disrupt clumps and 10ug/mL alpha factor was added, followed by 5ug/mL every hour until >95% cells were fully shmooed. After complete arrest, IAA was added and 5ug/mL alpha factor was added every hour to maintain arrest. To release cells from arrest, cells were washed twice with deionized water and resuspended in YPD with or without IAA as required.

Flow cytometry

Cells were collected by adding 150uL of yeast culture to 350uL absolute ethanol and stored at 4C. Samples were treated with RNase by pelleting cells and resuspending in 500uL of 50mM sodium citrate with 42ug/mL RNase A and incubating at 50C for two hours, followed by addition of 100ug

bioRxiv preprint doi: https://doi.org/10.1101/2019.12.17.879544; this version posted December 18, 2019. The copyright holder for this preprint (which was not certified by peer review) is the author/funder, who has granted bioRxiv a license to display the preprint in perpetuity. It is made available under aCC-BY-NC-ND 4.0 International license.

proteinase K for two additional hours. Equal volume of 50mM sodium citrate with 0.2uL SYTOX green (Fisher S7020) was added, samples were sonicated, and analyzed on a Becton Dickinson Accuri.

Subcellular fractionation and western blotting

Cells for subcellular fractionation were treated with 0.1% sodium azide and collected by centrifugation and stored at -20C. Cells were thawed on ice, washed and resuspended in spheroplasting buffer, and treated with 10uL of 20mg/mL zymolyase T20 and 1uL 1M DTT for 40 minutes at 30C before harvesting spheroplasts by centrifugation. Spheroplasts were resuspended in 300uL extraction buffer and divided into whole cell (50uL), soluble (50uL), and chromatin (200uL) fractions. The whole cell fraction was treated with 1.25uL 10% Triton-100, vortexed, incubated on ice for 5 minutes, treated with 1uL universal nuclease, incubated for 15 minutes on ice, and mixed with 20uL urea loading buffer. The soluble fraction was treated with 1.25uL 10% Triton-100, vortexed, incubated on ice for 5 minutes, centrifuged, and 20uL urea loading buffer was added to the supernatant. The chromatin fraction was treated with 1.25uL 10% Triton-100, vortexed and incubated on ice for 5 minutes before addition of 30% sucrose. After centrifugation, the previous step was repeated, and the resulting pellet was resuspended in 50µL EB with 1.25µL 10% Triton-100, treated with 1uL universal nuclease, incubated for 15 minutes on ice, and mixed with 20uL urea loading buffer.

Cells for western blotting were collected (2.0 OD units), washed, and resuspended in 200uL 20% TCA with glass beads, vortexed for 10 minutes, and the lysate was kept. The beads were washed with 600uL 5% TCA, combining with the lysate from the previous step. The lysate was centrifuged and the pellet was resuspended in 100uL urea loading buffer with 1uL 10M NaOH to restore color.

All western blotting samples were boiled for five minutes at 95C before loading onto an SDS-PAGE gel. Gels were blotted onto nitrocellulose membranes by wet transfer, blocked in 5% milk in PBS-T for one hour, and incubated with primary antibody at 4C overnight. After PBS-T washes, secondary antibody incubation for one hour, and PBS-T washes, blots were exposed with SuperSignal West Pico

bioRxiv preprint doi: https://doi.org/10.1101/2019.12.17.879544; this version posted December 18, 2019. The copyright holder for this preprint (which was not certified by peer review) is the author/funder, who has granted bioRxiv a license to display the preprint in perpetuity. It is made available under aCC-BY-NC-ND 4.0 International license.

(Fisher 34080). The following antibodies were used in this study: anti-myc (1:1000 Genscript A00173-100), anti-Rad53 (1:1000 Abcam ab104232), anti-S129phosp H2A (1:1000 Abcam ab15083), anti-Rfa1 (1:50000 Abcam ab221198), anti-H4 (1:1000 Abcam ab10158), anti-PGK1 (1:1000 Fisher 459250), anti-rabbit IgG HRP (1:5000 GE Healthcare NA934V), anti-mouse IgG HRP (1:5000 Abcam ab97046).

Okazaki fragment preparation, labeling and sequencing

Okazaki fragments were purified, end-labeled and deep-sequenced as previously described (7), with minor modifications. Briefly, Okazaki fragments were purified from genomic DNA collected after *CDC9* repression, using sequential elutions from Source 15Q columns. DNA was treated with RNase before adaptor ligation, second strand synthesis, and barcoding. Paired-end sequencing (2 × 75 bp) was carried out on an Illumina Next-seq 500 platform.

HydEN-seq

HydEN-seq was carried out as described (53). Briefly, DNA was cut with SbfI-HF, treated with 300mM KOH, and 5' phosphorylated before adapter ligation, second strand synthesis and barcoding. Paired-end sequencing (2 × 75 bp) was carried out on an Illumina Next-seq 500 platform

Computational analyses

FASTQ files were aligned to the S288C reference genome using the Bowtie (v2.2.9). Low quality reads and PCR duplicates were removed and resulting data was converted to BEDPE files using the Samtools suite (v1.3.1). For Okazaki fragment sequencing, genome coverage was calculated using the Bedtools suite (v2.26.0) in a strand-specific manner. Origin efficiency metric analysis of predefined origins was carried out as previously described (36) with the origin list from the same source (included as table S1). Briefly, the fraction of Okazaki fragments mapping to the Watson or Crick strand in 10 kb windows to the left and right of the origin (W_L, W_R, C_L, and C_R) is calculated for each origin. OEM is calculated as $W_L/(W_L+CL) – W_R/(W_R+C_R)$. Classification of origins as early or late was based on T_{rep}

bioRxiv preprint doi: https://doi.org/10.1101/2019.12.17.879544; this version posted December 18, 2019. The copyright holder for this preprint (which was not certified by peer review) is the author/funder, who has granted bioRxiv a license to display the preprint in perpetuity. It is made available under aCC-BY-NC-ND 4.0 International license.

from(37). Okazaki fragment ends were aligned to consensus nucleosome dyads (54) or Abf1/Reb1/Rap1 sites(55) and normalized to the median end density in a 2kb window around the sites.

DATA AVAILABILITY

Sequencing data have been submitted to the GEO under accession number 141884.

ACKNOWLEDGEMENTS

We thank Tom Petes and Dirk Remus for helpful discussions, and Hannah Klein for sharing strains. We thank members of the Smith lab for discussions and critical reading of the manuscript, and NYU Gencore for assistance with Illumina sequencing. This work was supported by NIH R01 GM114340 to D.J.S.

bioRxiv preprint doi: https://doi.org/10.1101/2019.12.17.879544; this version posted December 18, 2019. The copyright holder for this preprint (which was not certified by peer review) is the author/funder, who has granted bioRxiv a license to display the preprint in perpetuity. It is made available under aCC-BY-NC-ND 4.0 International license.

LEGENDS TO FIGURES

Figure 1. Titration of Pol3 *in vivo* delays and extends S-phase, leading to slow growth

A. Western blot against Pol3-9Myc in asynchronous cultures of the *POL3-AID* strain following 2h of treatment with the indicated concentration of IAA. Myc-tagged TIR1 is required for degradation of Pol3, and serves as a loading control.

B. Serial dilution spot tests of *POL3-AID* cells and two control strains on YPD plates supplemented with IAA at concentrations from 0 to 1 mM.

C. DNA content measured by flow cytometry for *POL3-AID* cells released from α-factor-mediated G1 arrest at 30˚C. Individual cultures were treated with the indicated concentration of IAA for 2h during the initial arrest, and subsequently released into media containing the same concentration of IAA.

Figure 2. Pol3 depletion leads to DNA damage, checkpoint activation and RPA accumulation on chromatin

A. Western blots to detect Rad53 phosphorylation in asynchronous cultures of the indicated strains grown in YPD supplemented with IAA.

B. Serial dilution spot tests of *POL3-AID* cells with the indicated additional mutations on YPD plates supplemented with IAA at concentrations from 0 to 1 mM.

C. Serial dilution spot tests of *POL3-AID* or *POL3-AID;mec1Δ;sml1Δ* cells exposed to 1 mM IAA for 0, 2 or 4h of growth during logarithmic phase, followed by plating on YPD without IAA.

D. DNA content measured by flow cytometry for *POL3-AID* or *POL3-AID;mec1Δ;sml1Δ* cells released from α-factor-mediated G1 arrest at 30˚C. As in Fig. 1C, individual cultures were treated with the indicated concentration of IAA for 2h during the initial arrest, and subsequently released into media containing the same concentration of IAA.

E. Western blot to detect histone H2A phosphorylation at S129 in asynchronous cultures of the *POL3-AID* strain grown in YPD supplemented with IAA as indicated.

F. Serial dilution spot tests of *POL3-AID* cells with the indicated additional mutations on YPD plates supplemented with IAA at concentrations from 0 to 1 mM.

bioRxiv preprint doi: https://doi.org/10.1101/2019.12.17.879544; this version posted December 18, 2019. The copyright holder for this preprint (which was not certified by peer review) is the author/funder, who has granted bioRxiv a license to display the preprint in perpetuity. It is made available under aCC-BY-NC-ND 4.0 International license.

G. Western blot against Rfa1 on soluble and chromatin-bound fractions of log-phase *POL3-AID* cells treated with the indicated IAA concentration for 2h.

H. Western blots as in (G), but using cells collected during G1 arrest, or in mid- or late S-phase as indicated.

Figure 3. Pol3 depletion decreases firing efficiency of early replication origins, but increases firing efficiency of late origins.

A. Okazaki fragment sequencing data across chromosome 7 for asynchronous *POL3-AID* cultures treated with the indicated concentration of IAA for 2h before and during 1h rapamycin treatment to deplete Cdc9 from the nucleus by anchor away. Watson-strand fragments deriving from leftward-moving forks are shown above the axis, and Crick-strand fragments deriving from rightward forks below the axis.

B. Replication-origin firing efficiency in *POL3-AID*, calculated as OEM from Okazaki fragment distributions around 281 high-confidence origins (36). Data in panels B-E represent the mean efficiency averaged across two replicate strains at each concentration of IAA. Equivalent data for individual replicates are shown in Fig. S2. Whiskers indicate 5^{th}-95^{th} percentile, with outliers as points. $p < 0.0001$ by Kolmogorov-Smirnov test for a change in distribution between 0 and 1 mM.

C. Scatter plot comparing origin efficiency in YPD ±1 mM IAA. The line of identity is shown in red.

D-E. As for B, but for (D) early- or (E) late-firing origins, defined as those with a T_{rep} (37) below or above the median for the set of origins analyzed, respectively. $p < 0.0001$ by Wilcoxon signed rank test for a change in mean between 0 and 1 mM in both cases.

Figure 4. Pol3 depletion slows replication fork progression

A. Okazaki fragment sequencing data across chromosome 10 for cultures released from α-factor-mediated G1 arrest at 25˚C. IAA treatment during and following arrest was maintained as in Fig. 1C and 2D. Watson and Crick strand data are displayed as in Fig. 3A. Time points shown in color are analyzed in B and C. Flow cytometry data for this experiment are in Fig. S3

bioRxiv preprint doi: https://doi.org/10.1101/2019.12.17.879544; this version posted December 18, 2019. The copyright holder for this preprint (which was not certified by peer review) is the author/funder, who has granted bioRxiv a license to display the preprint in perpetuity. It is made available under aCC-BY-NC-ND 4.0 International license.

B. Total coverage of Okazaki fragments on both the Watson and Crick strands across a 40 kb region around early-firing origins (defined as in Fig. 3D) at the indicated time and concentration of IAA. Data are shown with a 100 bp bin size, and are normalized to the maximum signal in the range such that complete replication will result in a flat line at 1.0.

C. Coverage of Watson-strand Okazaki fragments in the region from -20 kb to -1 kb, and Crick-strand Okazaki fragments in the region from +1 kb to +20 kb around the early-firing origins analyzed in B. This analysis specifically measures the progression of leftward- and rightward-moving forks emanating from these origins. As in B, data are normalized to the maximum signal in the entire 40 kb range.

Figure 5. Pol3 depletion impairs normal Okazaki fragment processing

A. End-labeled Okazaki fragments from asynchronous *POL3-AID* cultures treated with the indicated concentration of IAA for 2h before and during 1h rapamycin treatment to deplete Cdc9 from the nucleus by anchor away. Fragments were labeled with [α-^{32}P] dCTP and Klenow exo$^-$, as described in the methods.

B-C. Distribution of Okazaki fragment 5' and 3' ends around the midpoints of (B) high-confidence nucleosomes (54) and (C) Abf1/Reb1/Rap1 sites (55). Data are smoothed to 5 bp and normalized to the median value in the range ±1000 bp from the nucleosome or transcription-factor binding site midpoint. Data from one of two replicates are shown; the other replicate is in Fig. S4C-D.

Figure 6. Pol ε can participate in lagging-strand synthesis in late-replicating regions when Pol ∂ is limiting

A. Serial dilution spot tests of *POL3-AID* cells with the indicated additional mutations on YPD plates supplemented with IAA at concentrations from 0 to 1 mM.

B. Schematic showing the expected change in ribonucleotide incorporation around a meta-replication origin by Pol ε in scenarios where Pol ε synthesizes some or all of the lagging strand.

bioRxiv preprint doi: https://doi.org/10.1101/2019.12.17.879544; this version posted December 18, 2019. The copyright holder for this preprint (which was not certified by peer review) is the author/funder, who has granted bioRxiv a license to display the preprint in perpetuity. It is made available under aCC-BY-NC-ND 4.0 International license.

C. Fraction of ribonucleotides identified by HydEn-seq (11) mapping to the Watson strand around the same set of replication origins analyzed in Fig. 3B. Asynchronous culture of the *POL3-AID;pol2-M644G;rnh202Δ* strain was treated ±1 mM IAA for 2h prior to cell collection. Data shown are the average of two biological replicates. Data for individual replicates are in Fig. S5.

D-E. Change in the fraction of ribonucleotides mapping to the Watson strand (red) and Okazaki fragments mapping to the Crick strand (black) around early (D) or late (E) replication origins (defined as in Fig. 3D&E). Okazaki fragment polarity data are the same as used in Fig. 3, and represent the average of the two replicates. The polarities are chosen such that altered ribonucleotide distribution resulting from a change in replication origin efficiency will produce overlapping lines.

F. Inferred contribution of Pol ε to lagging-strand synthesis around early (grey) and late (blue) replication origins. Values are calculated by subtracting the change in fork polarity from the change in ribonucleotide incorporation and reversing the sign for the region upstream of the meta-origin.

Figure 7. Model

A. Under normal conditions, at least two Pol ∂ complexes are available at the replication fork. This allows the simultaneous processing of one Okazaki fragment and extension of the subsequent primer.

B. Under conditions of Pol ∂ depletion, the two substrates compete for a single Pol ∂. Either (i) extension of Pol α-derived primers (orange) or (ii) nick translation on the terminating Okazaki fragment is impaired, leading to the phenotypes outlined in each scenario. Our data are consistent with both (i) and (ii) occurring for at least a fraction of replisomes.

bioRxiv preprint doi: https://doi.org/10.1101/2019.12.17.879544; this version posted December 18, 2019. The copyright holder for this preprint (which was not certified by peer review) is the author/funder, who has granted bioRxiv a license to display the preprint in perpetuity. It is made available under aCC-BY-NC-ND 4.0 International license.

Koussa and Smith, Figure 1

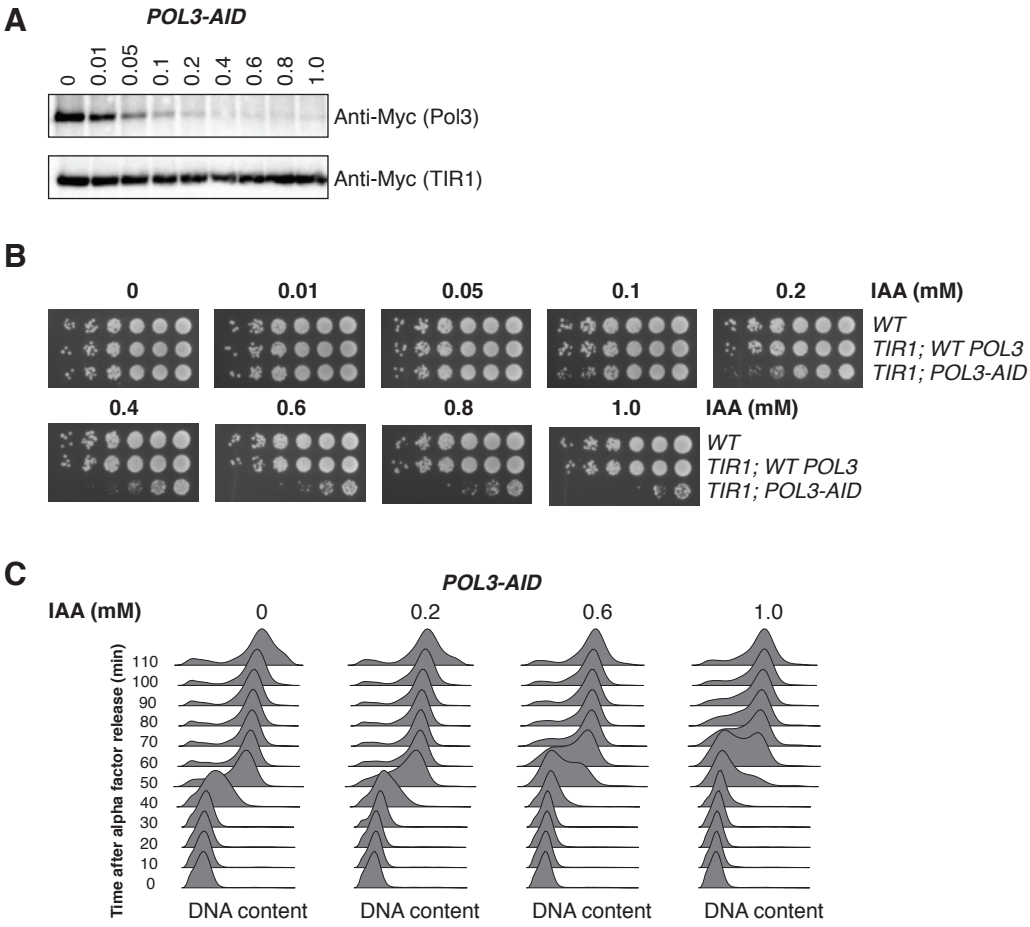

bioRxiv preprint doi: https://doi.org/10.1101/2019.12.17.879544; this version posted December 18, 2019. The copyright holder for this preprint (which was not certified by peer review) is the author/funder, who has granted bioRxiv a license to display the preprint in perpetuity. It is made available under aCC-BY-NC-ND 4.0 International license.

Koussa and Smith, Figure 2

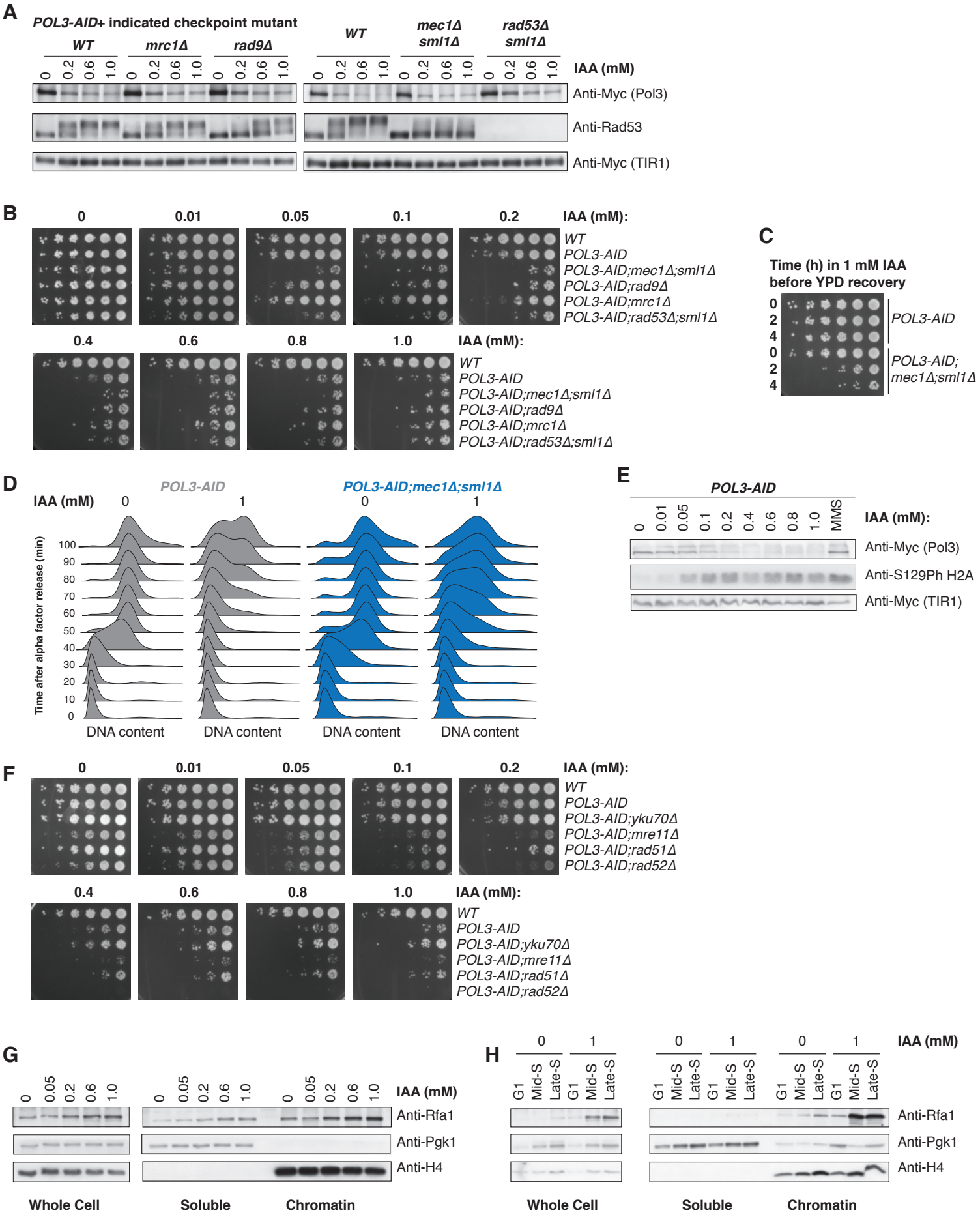

bioRxiv preprint doi: https://doi.org/10.1101/2019.12.17.879544; this version posted December 18, 2019. The copyright holder for this preprint (which was not certified by peer review) is the author/funder, who has granted bioRxiv a license to display the preprint in perpetuity. It is made available under aCC-BY-NC-ND 4.0 International license.

Koussa and Smith, Figure 3

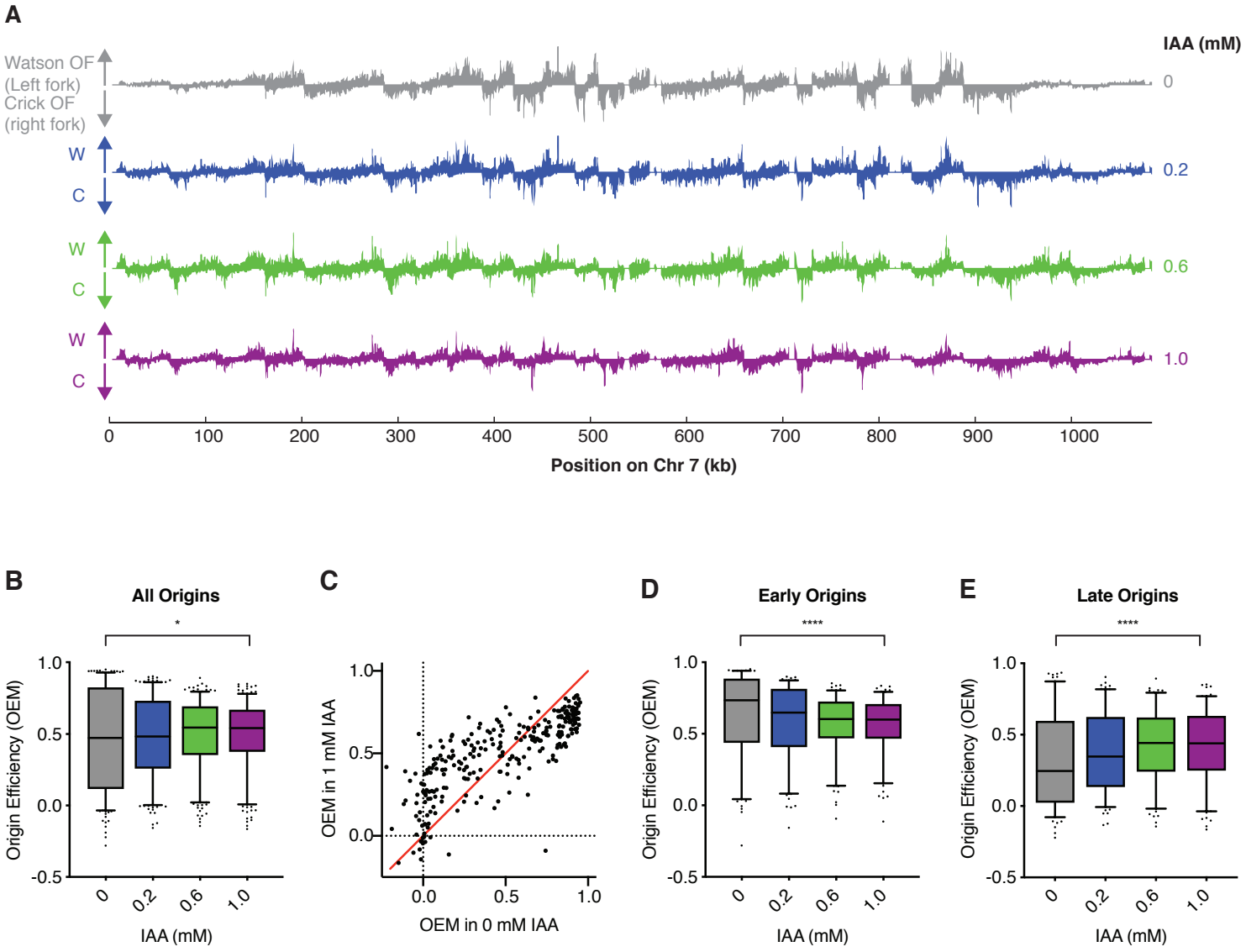

bioRxiv preprint doi: https://doi.org/10.1101/2019.12.17.879544; this version posted December 18, 2019. The copyright holder for this preprint (which was not certified by peer review) is the author/funder, who has granted bioRxiv a license to display the preprint in perpetuity. It is made available under aCC-BY-NC-ND 4.0 International license.

Koussa and Smith, Figure 4

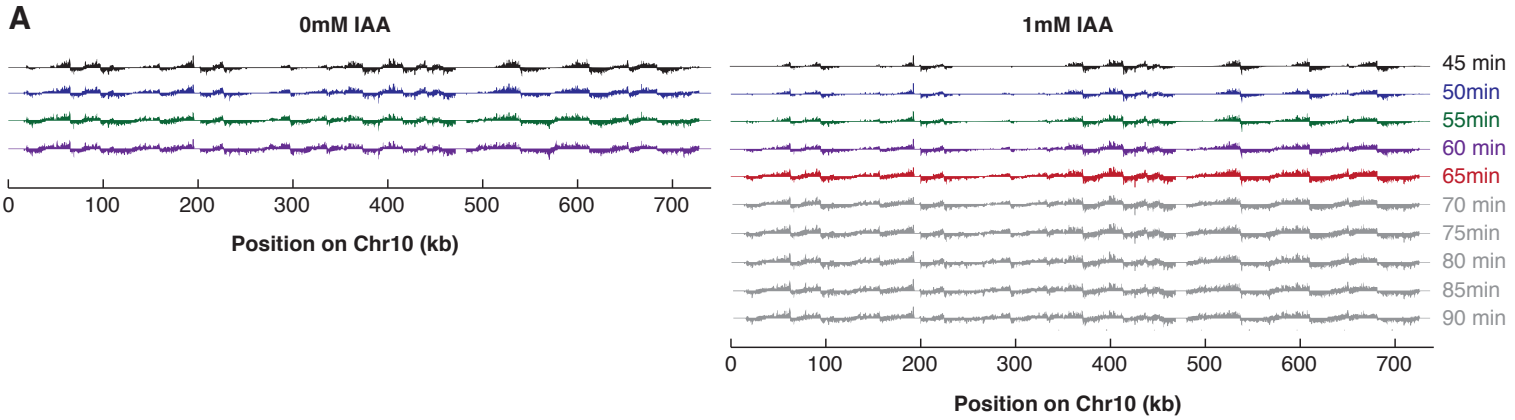

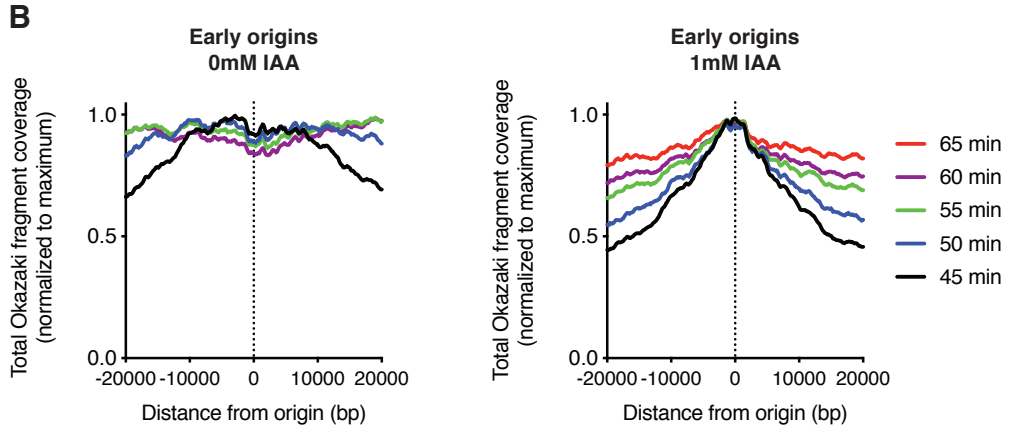

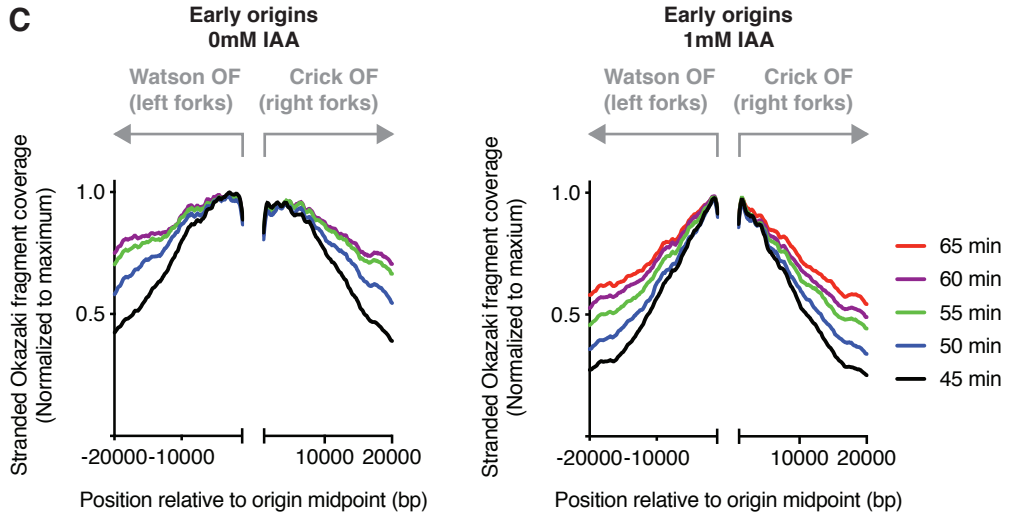

bioRxiv preprint doi: https://doi.org/10.1101/2019.12.17.879544; this version posted December 18, 2019. The copyright holder for this preprint (which was not certified by peer review) is the author/funder, who has granted bioRxiv a license to display the preprint in perpetuity. It is made available under aCC-BY-NC-ND 4.0 International license.

Koussa and Smith, Figure 5

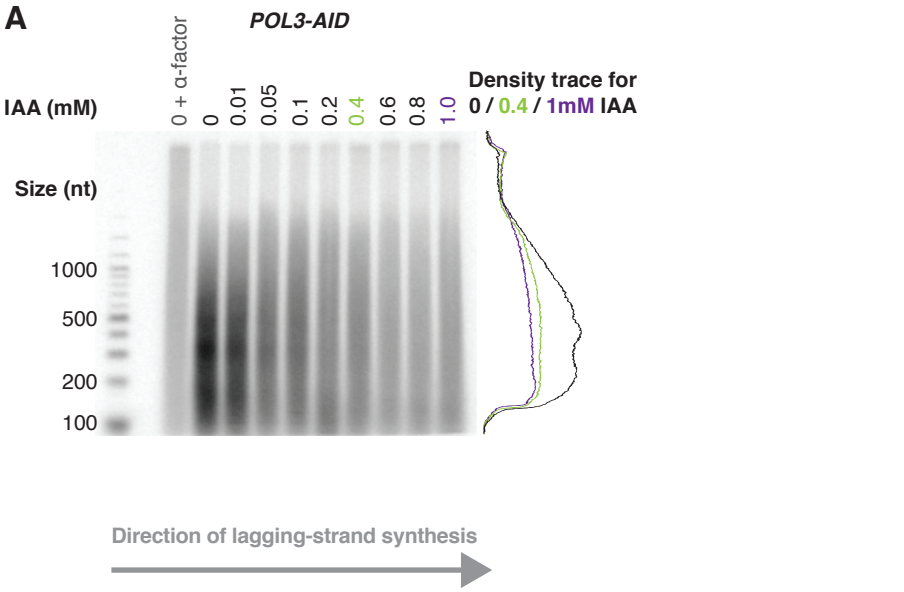

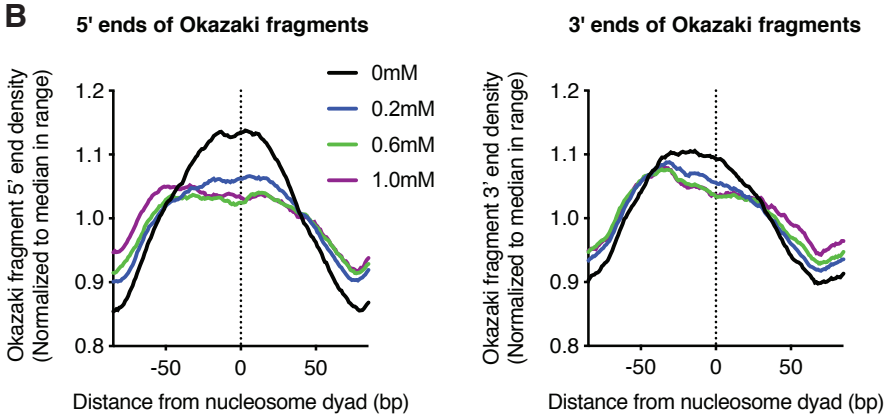

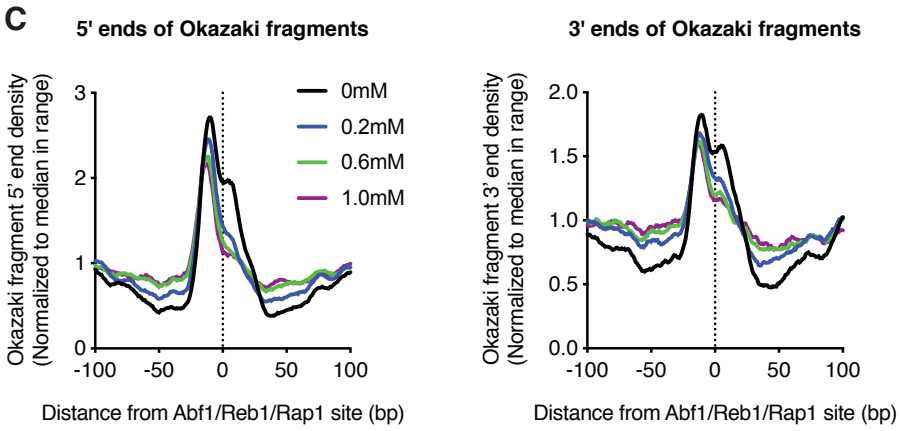

bioRxiv preprint doi: https://doi.org/10.1101/2019.12.17.879544; this version posted December 18, 2019. The copyright holder for this preprint (which was not certified by peer review) is the author/funder, who has granted bioRxiv a license to display the preprint in perpetuity. It is made available under aCC-BY-NC-ND 4.0 International license.

Koussa and Smith, Figure 6

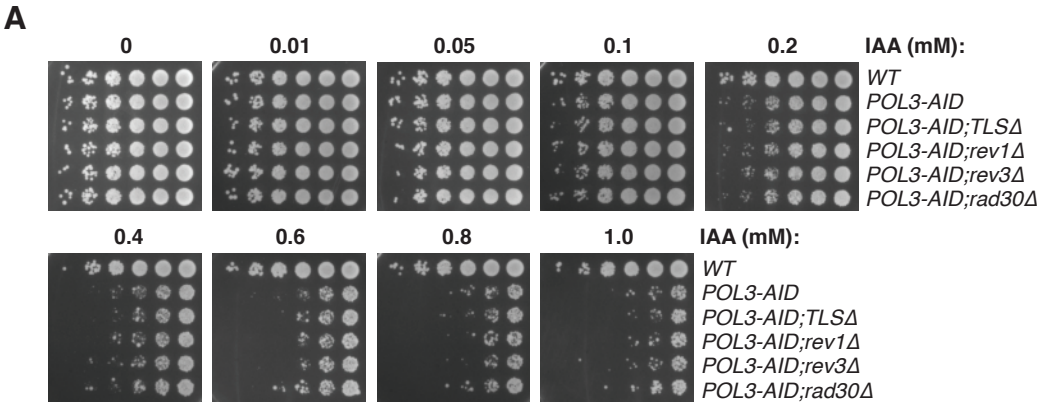

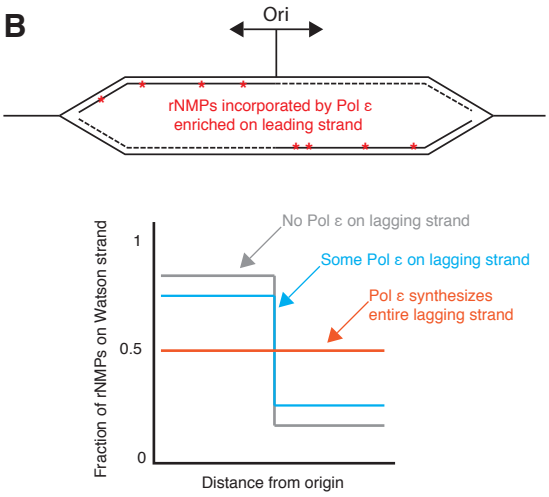

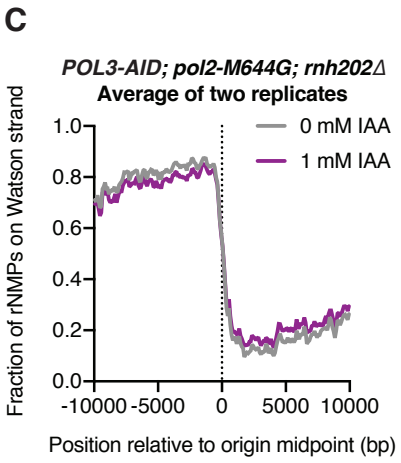

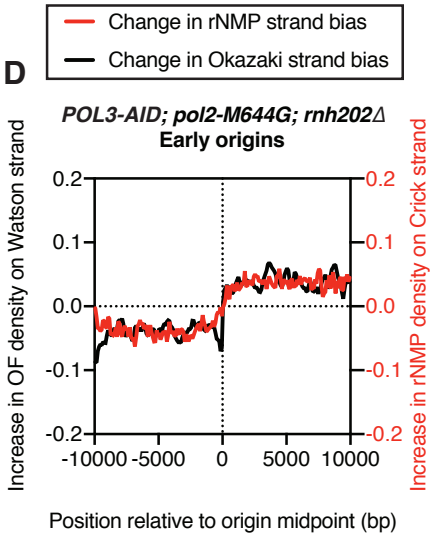

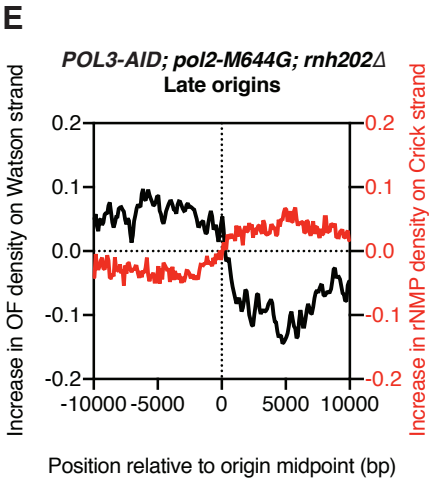

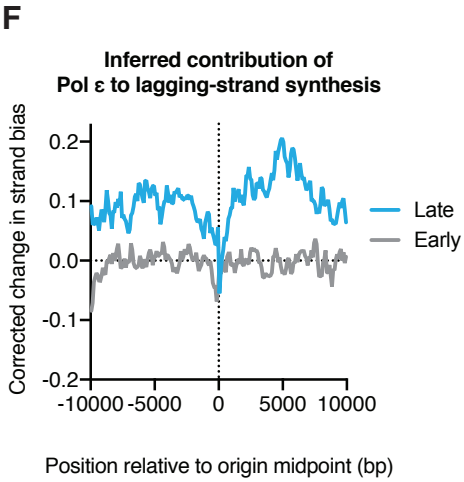

bioRxiv preprint doi: https://doi.org/10.1101/2019.12.17.879544; this version posted December 18, 2019. The copyright holder for this preprint (which was not certified by peer review) is the author/funder, who has granted bioRxiv a license to display the preprint in perpetuity. It is made available under aCC-BY-NC-ND 4.0 International license.

Koussa and Smith, Figure 7

A

Abundant Pol ∂. At least two Pol ∂ available per replisome.

Efficient, concurrent Okazaki fragment processing and extension of newly synthesized Pol α primers.

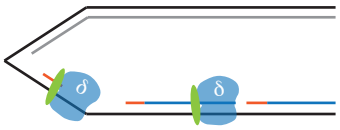

B

Pol ∂ depletion or hypomorphy. Many replisomes with fewer than two avaiable Pol ∂.

Terminating and nascent Okazaki fragments compete for a single Pol ∂.

(i)

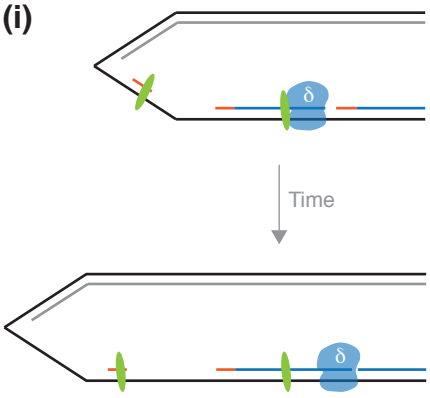

Pol ∂ participates in Okazaki fragment processing.
Pol α primers unextended for long periods.
ssDNA accumulates; replication fork slows.
Single-stranded gaps accumulate?

(ii)

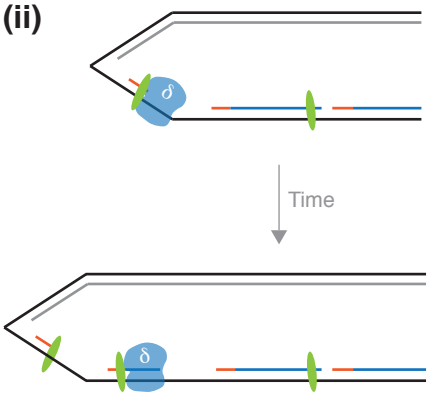

Pol ∂ extends Pol α primers.
Okazaki fragment processing impaired.
Partially processed OF intermediates accumulate.
Retention of un-proofread DNA from Pol α synthesis.

bioRxiv preprint doi: https://doi.org/10.1101/2019.12.17.879544; this version posted December 18, 2019. The copyright holder for this preprint (which was not certified by peer review) is the author/funder, who has granted bioRxiv a license to display the preprint in perpetuity. It is made available under aCC-BY-NC-ND 4.0 International license.

LEGENDS TO SUPPLEMENTARY FIGURES

Supplementary figure 1 (associated with figure 1).

Further characterization of Pol3 depletion kinetics and the effect of depletion on growth rate.

A. Western blot against Pol3-9Myc or TIR1-9Myc in asynchronous cultures of the *POL3-AID* strain following 30 minutes of treatment with the indicated concentration of IAA

B. Growth rates of *POL3-AID* cells in liquid culture. Data were calculated from three replicates.

C. DNA content measured by flow cytometry for logarithmically growing *POL3-AID* cells treated with the indicated concentration of IAA for 2h

Supplementary figure 2 (associated with figure 3).

Effects of Pol3 depletion on replication origin firing in individual replicates.

A-F. Analysis of replication origin firing efficiency as shown for pooled replicates in Fig. 3B,D&E, separated by individual biological replicate strain as indicated. **** denotes $p < 0.0001$ by Kolmogorov-Smirnov test (A,D) or Wilcoxon signed rank test (B-C, E-F) for a change in the distribution or mean of the data, respectively.

Supplementary figure 3 (associated with figure 4)

Samples used for analysis of replication-fork speed in figure 4.

DNA content measured by flow cytometry for the samples shown in Fig. 4A. Red timepoints were sequenced for both 0 and 1 mM IAA, and blue timepoints for 1 mM only.

Supplementary figure 4 (associated with figure 5)

Additional analysis of the effects of Pol3 depletion on lagging-strand synthesis and processing.

A. Representative replicate analysis for the Okazaki fragment labeling experiment shown in Fig. 5A

B. Okazaki fragment labeling experiment as in Fig. 5A and S4A, but in an *POL3-AID* strain.

bioRxiv preprint doi: https://doi.org/10.1101/2019.12.17.879544; this version posted December 18, 2019. The copyright holder for this preprint (which was not certified by peer review) is the author/funder, who has granted bioRxiv a license to display the preprint in perpetuity. It is made available under aCC-BY-NC-ND 4.0 International license.

C-D. Distribution of Okazaki fragment 5' and 3' ends around (C) nucleosomes and (D) Abf1/Reb1/Rap1 sites as in Fig. 5B-C, for the other biological replicate

Supplementary figure 5 (associated with figure 6).

Effects of Pol3 depletion on the strand specificity of ribonucleotide incorporation by Pol ε.

A-H. Analysis of ribonucleotide distribution around replication origins in the *POL3-AID;pol2-M644G;rnh202Δ* genetic background as shown for pooled replicates in Fig. 6C-E, separated by individual biological replicate strain as indicated.

Supplementary figure 6 (associated with figure 6).

Lagging-strand processing is impaired in both early- and late-replicating regions of the genome during Pol3 depletion.

A-B. Distribution of Okazaki fragment 5' and 3' ends around nucleosomes within 10 kb of an early-firing replication origin (early) or 10 kb of a late-firing origin (late) for the two biological replicates shown in figures 5 and S4.

bioRxiv preprint doi: https://doi.org/10.1101/2019.12.17.879544; this version posted December 18, 2019. The copyright holder for this preprint (which was not certified by peer review) is the author/funder, who has granted bioRxiv a license to display the preprint in perpetuity. It is made available under aCC-BY-NC-ND 4.0 International license.

Koussa and Smith, Figure S1

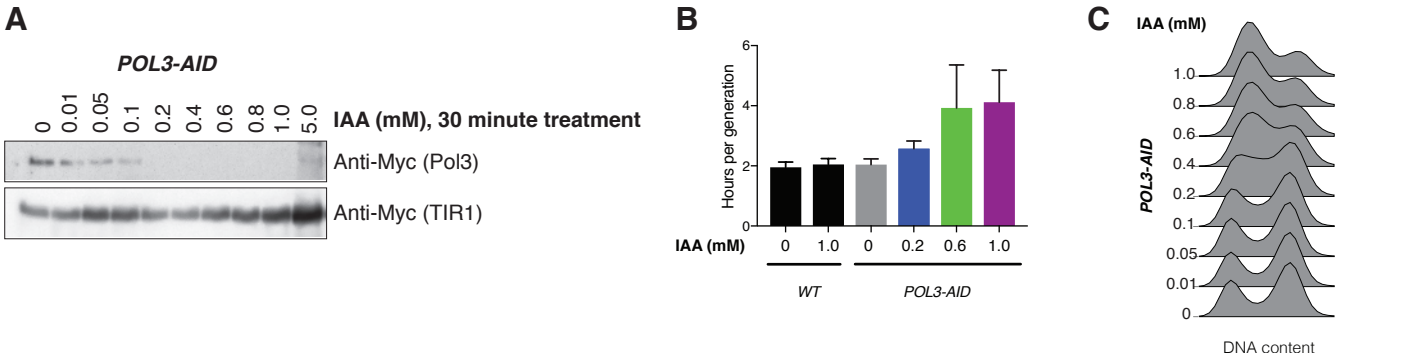

bioRxiv preprint doi: https://doi.org/10.1101/2019.12.17.879544; this version posted December 18, 2019. The copyright holder for this preprint (which was not certified by peer review) is the author/funder, who has granted bioRxiv a license to display the preprint in perpetuity. It is made available under aCC-BY-NC-ND 4.0 International license.

Koussa and Smith, Figure S2

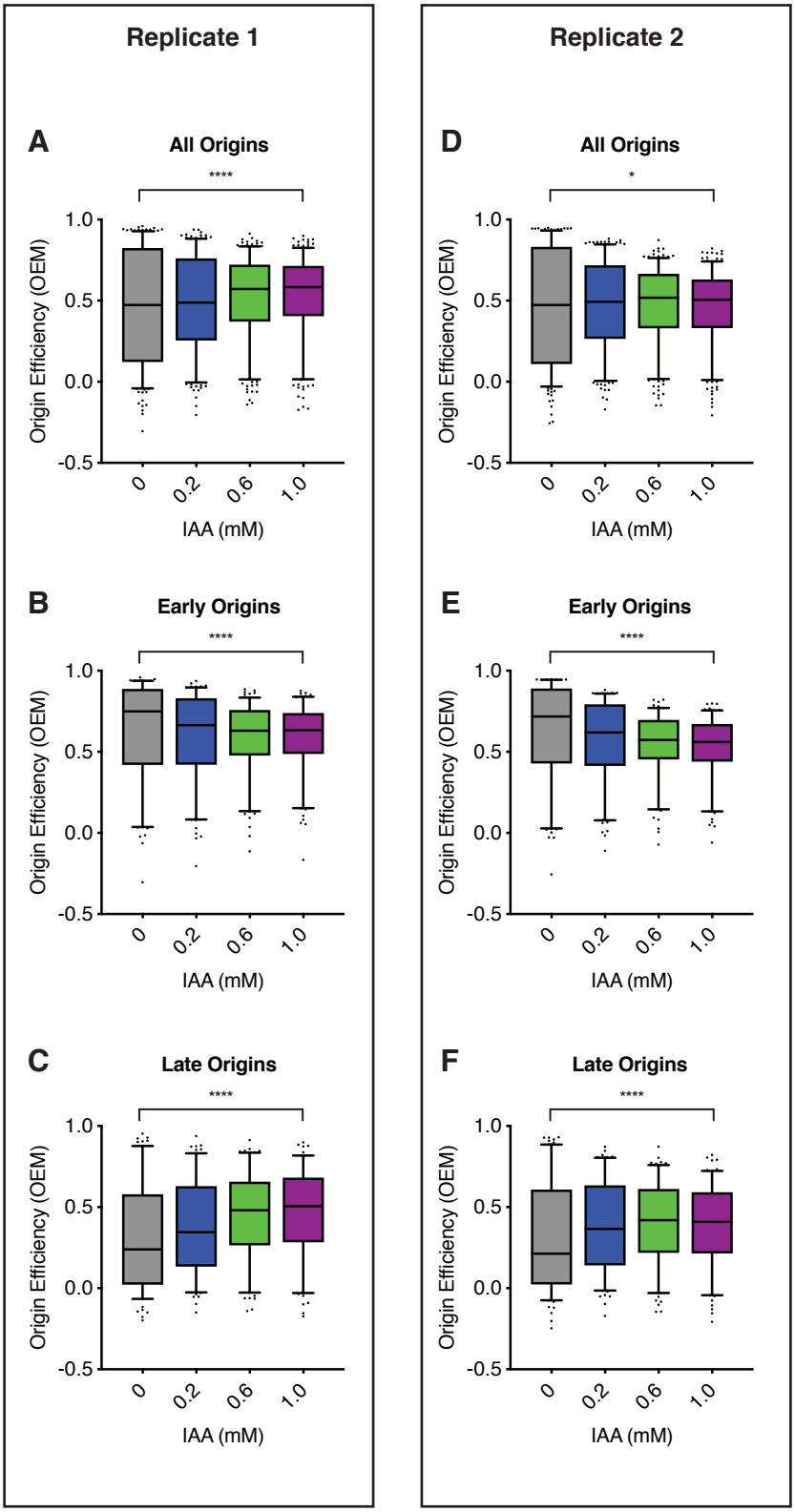

bioRxiv preprint doi: https://doi.org/10.1101/2019.12.17.879544; this version posted December 18, 2019. The copyright holder for this preprint (which was not certified by peer review) is the author/funder, who has granted bioRxiv a license to display the preprint in perpetuity. It is made available under aCC-BY-NC-ND 4.0 International license.

Koussa and Smith, Figure S3

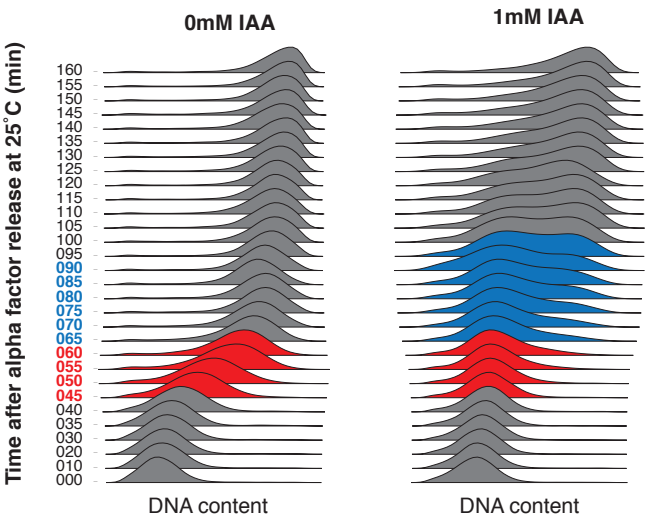

bioRxiv preprint doi: https://doi.org/10.1101/2019.12.17.879544; this version posted December 18, 2019. The copyright holder for this preprint (which was not certified by peer review) is the author/funder, who has granted bioRxiv a license to display the preprint in perpetuity. It is made available under aCC-BY-NC-ND 4.0 International license.

Koussa and Smith, Figure S4

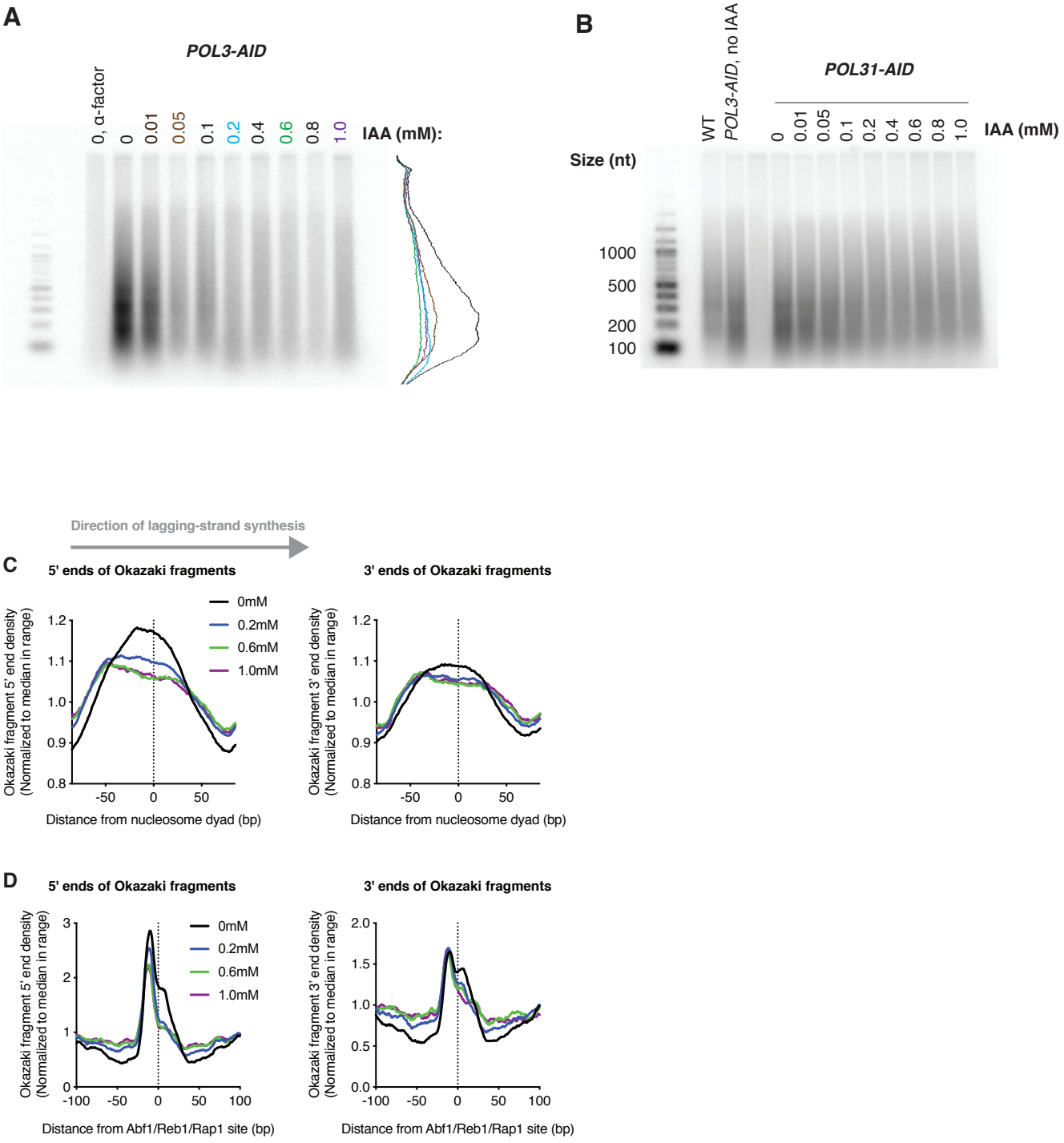

bioRxiv preprint doi: https://doi.org/10.1101/2019.12.17.879544; this version posted December 18, 2019. The copyright holder for this preprint (which was not certified by peer review) is the author/funder, who has granted bioRxiv a license to display the preprint in perpetuity. It is made available under aCC-BY-NC-ND 4.0 International license.

Koussa and Smith, Figure S5

POL3-AID; pol2-M644G; rnh202Δ

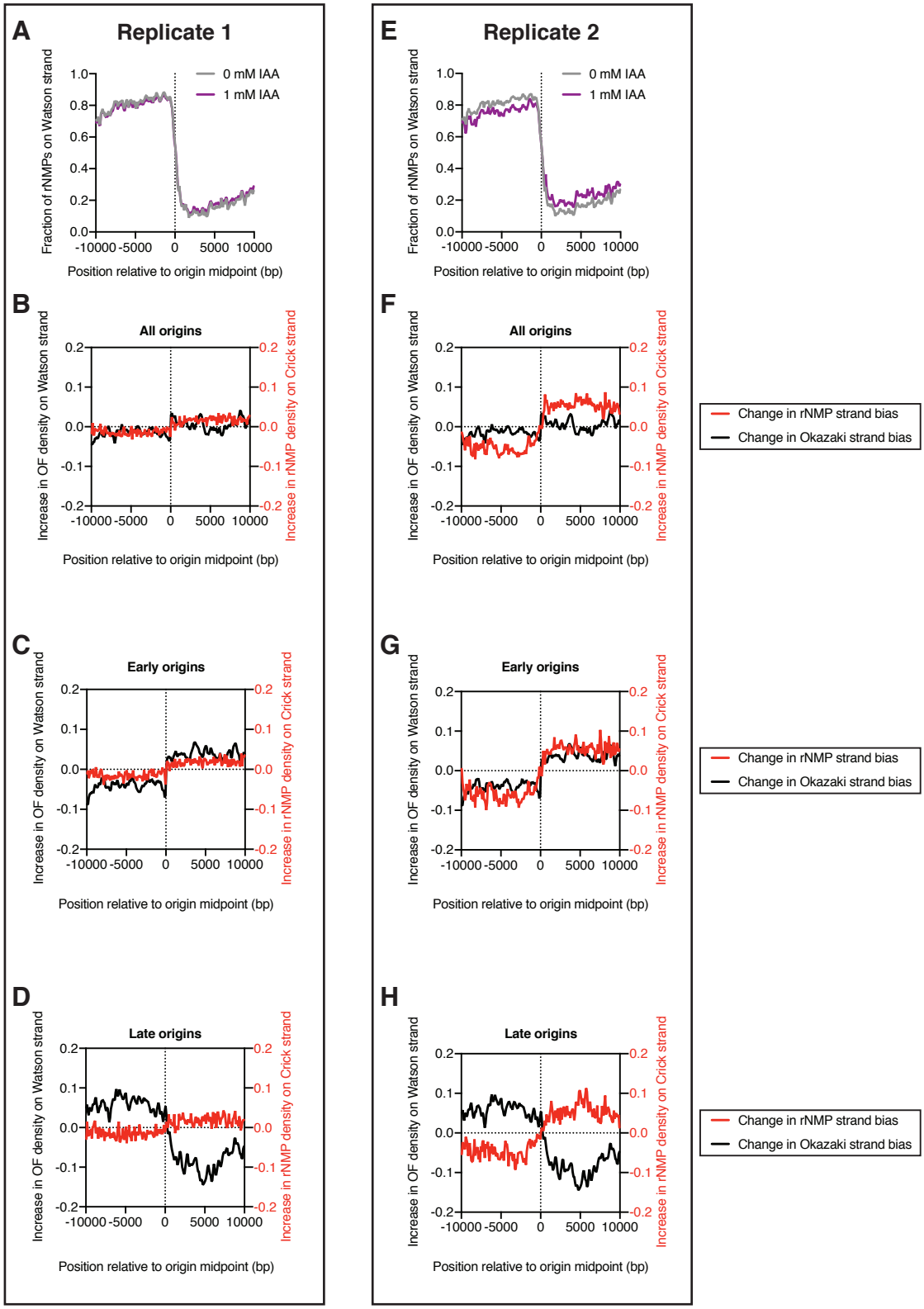

bioRxiv preprint doi: https://doi.org/10.1101/2019.12.17.879544; this version posted December 18, 2019. The copyright holder for this preprint (which was not certified by peer review) is the author/funder, who has granted bioRxiv a license to display the preprint in perpetuity. It is made available under aCC-BY-NC-ND 4.0 International license.

Koussa and Smith, Figure S6

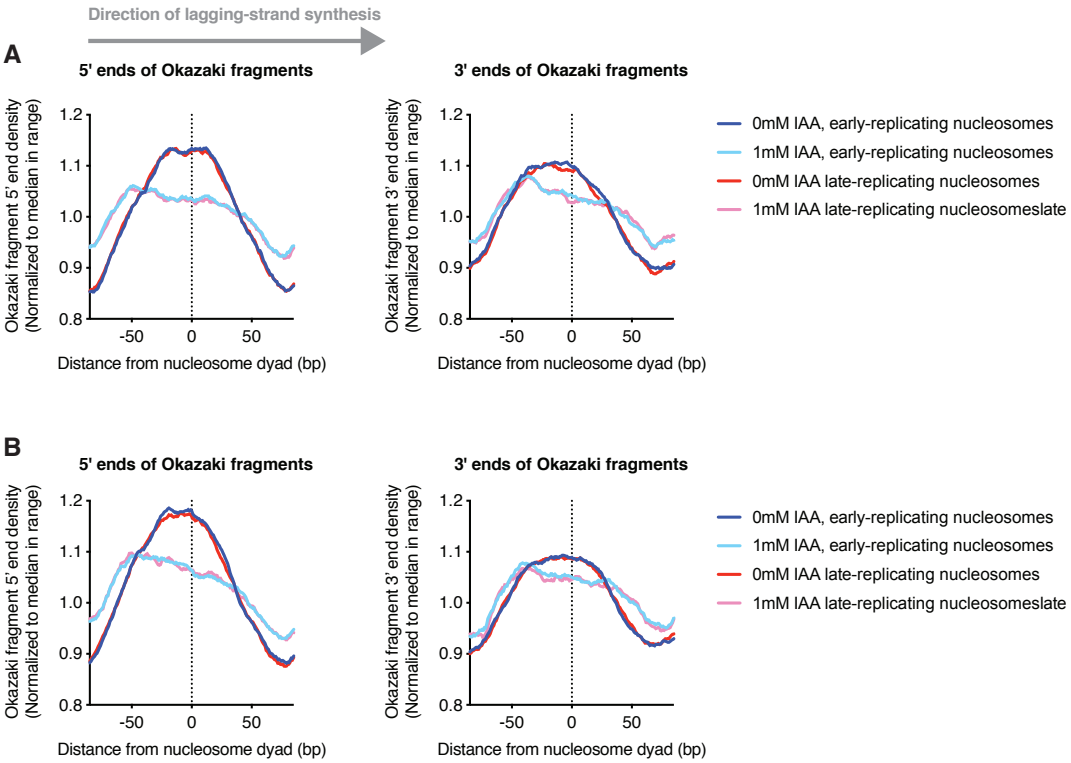

bioRxiv preprint doi: https://doi.org/10.1101/2019.12.17.879544; this version posted December 18, 2019. The copyright holder for this preprint (which was not certified by peer review) is the author/funder, who has granted bioRxiv a license to display the preprint in perpetuity. It is made available under aCC-BY-NC-ND 4.0 International license.

REFERENCES

1. Burgers, P. M. 2009. Polymerase dynamics at the eukaryotic DNA replication fork. *J Biol Chem* 284: 4041-4045.
2. Balakrishnan, L., and R. A. Bambara. 2013. Okazaki fragment metabolism. *Cold Spring Harb Perspect Biol* 5:; doi: 10.1101/cshperspect.a010173.
3. Ayyagari, R., X. V. Gomes, D. A. Gordenin, and P. M. Burgers. 2003. Okazaki fragment maturation in yeast. I. Distribution of functions between FEN1 AND DNA2. *J Biol Chem* 278: 1618-1625.
4. Garg, P., C. M. Stith, N. Sabouri, E. Johansson, and P. M. Burgers. 2004. Idling by DNA polymerase delta maintains a ligatable nick during lagging-strand DNA replication. *Genes Dev* 18: 2764-2773.
5. Stodola, J. L., and P. M. Burgers. 2016. Resolving individual steps of Okazaki-fragment maturation at a millisecond timescale. *Nat Struct Mol Biol* 23: 402-408.
6. Kahli, M., J. S. Osmundson, R. Yeung, and D. J. Smith. 2019. Processing of eukaryotic Okazaki fragments by redundant nucleases can be uncoupled from ongoing DNA replication in vivo. *Nucleic Acids Res* 47: 1814-1822.
7. Smith, D. J., and I. Whitehouse. 2012. Intrinsic coupling of lagging-strand synthesis to chromatin assembly. *Nature* 483: 434-438.
8. Aria, V., and J. T. P. Yeeles. 2018. Mechanism of Bidirectional Leading-Strand Synthesis Establishment at Eukaryotic DNA Replication Origins. *Mol Cell*
9. Garbacz, M. A., S. A. Lujan, A. B. Burkholder, P. B. Cox, Q. Wu, Z. X. Zhou, J. E. Haber, and T. A. Kunkel. 2018. Evidence that DNA polymerase δ contributes to initiating leading strand DNA replication in Saccharomyces cerevisiae. *Nat Commun* 9: 858.
10. Yeeles, J. T., A. Janska, A. Early, and J. F. Diffley. 2017. How the Eukaryotic Replisome Achieves Rapid and Efficient DNA Replication. *Mol Cell* 65: 105-116.

bioRxiv preprint doi: https://doi.org/10.1101/2019.12.17.879544; this version posted December 18, 2019. The copyright holder for this preprint (which was not certified by peer review) is the author/funder, who has granted bioRxiv a license to display the preprint in perpetuity. It is made available under aCC-BY-NC-ND 4.0 International license.

11. Clausen, A. R., S. A. Lujan, A. B. Burkholder, C. D. Orebaugh, J. S. Williams, M. F. Clausen, E. P. Malc, P. A. Mieczkowski, D. C. Fargo, D. J. Smith, and T. A. Kunkel. 2015. Tracking replication enzymology in vivo by genome-wide mapping of ribonucleotide incorporation. *Nat Struct Mol Biol* 22: 185-191.

12. Daigaku, Y., A. Keszthelyi, C. A. Muller, I. Miyabe, T. Brooks, R. Retkute, M. Hubank, C. A. Nieduszynski, and A. M. Carr. 2015. A global profile of replicative polymerase usage. *Nat Struct Mol Biol* 22: 192-198.

13. Georgescu, R. E., L. Langston, N. Y. Yao, O. Yurieva, D. Zhang, J. Finkelstein, T. Agarwal, and M. E. O'Donnell. 2014. Mechanism of asymmetric polymerase assembly at the eukaryotic replication fork. *Nat Struct Mol Biol* 21: 664-670.

14. Georgescu, R. E., G. D. Schauer, N. Y. Yao, L. D. Langston, O. Yurieva, D. Zhang, J. Finkelstein, and M. E. O'Donnell. 2015. Reconstitution of a eukaryotic replisome reveals suppression mechanisms that define leading/lagging strand operation. *Elife* 4:

15. Devbhandari, S., J. Jiang, C. Kumar, I. Whitehouse, and D. Remus. 2017. Chromatin Constrains the Initiation and Elongation of DNA Replication. *Mol Cell* 65: 131-141.

16. Feng, W., and G. D'Urso. 2001. Schizosaccharomyces pombe cells lacking the amino-terminal catalytic domains of DNA polymerase epsilon are viable but require the DNA damage checkpoint control. *Mol Cell Biol* 21: 4495-4504.

17. Kesti, T., K. Flick, S. Keranen, J. E. Syvaoja, and C. Wittenberg. 1999. DNA polymerase epsilon catalytic domains are dispensable for DNA replication, DNA repair, and cell viability. *Mol Cell* 3: 679-685.

18. Zhou, Z. X., S. A. Lujan, A. B. Burkholder, M. A. Garbacz, and T. A. Kunkel. 2019. Roles for DNA polymerase δ in initiating and terminating leading strand DNA replication. *Nat Commun* 10: 3992.

bioRxiv preprint doi: https://doi.org/10.1101/2019.12.17.879544; this version posted December 18, 2019. The copyright holder for this preprint (which was not certified by peer review) is the author/funder, who has granted bioRxiv a license to display the preprint in perpetuity. It is made available under aCC-BY-NC-ND 4.0 International license.

19. Goldsby, R. E., L. E. Hays, X. Chen, E. A. Olmsted, W. B. Slayton, G. J. Spangrude, and B. D. Preston. 2002. High incidence of epithelial cancers in mice deficient for DNA polymerase delta proofreading. *Proc Natl Acad Sci U S A* 99: 15560-15565.

20. Heitzer, E., and I. Tomlinson. 2014. Replicative DNA polymerase mutations in cancer. *Curr Opin Genet Dev* 24: 107-113.

21. Venkatesan, R. N., P. M. Treuting, E. D. Fuller, R. E. Goldsby, T. H. Norwood, T. A. Gooley, W. C. Ladiges, B. D. Preston, and L. A. Loeb. 2007. Mutation at the polymerase active site of mouse DNA polymerase delta increases genomic instability and accelerates tumorigenesis. *Mol Cell Biol* 27: 7669-7682.

22. Daee, D. L., T. M. Mertz, and P. V. Shcherbakova. 2009. A cancer-associated DNA polymerase {delta} variant modeled in yeast causes a catastrophic increase in genomic instability. *Proc Natl Acad Sci U S A*

23. Weedon, M. N., S. Ellard, M. J. Prindle, R. Caswell, H. L. Allen, R. Oram, K. Godbole, C. S. Yajnik, P. Sbraccia, G. Novelli, P. Turnpenny, E. McCann, K. J. Goh, Y. Wang, J. Fulford, L. J. McCulloch, D. B. Savage, S. O'Rahilly, K. Kos, L. A. Loeb, R. K. Semple, and A. T. Hattersley. 2013. An in-frame deletion at the polymerase active site of POLD1 causes a multisystem disorder with lipodystrophy. *Nat Genet*

24. Conde, C. D., Ö. Y. Petronczki, S. Baris, K. L. Willmann, E. Girardi, E. Salzer, S. Weitzer, R. C. Ardy, A. Krolo, H. Ijspeert, A. Kiykim, E. Karakoc-Aydiner, E. Förster-Waldl, L. Kager, W. F. Pickl, G. Superti-Furga, J. Martínez, J. I. Loizou, A. Ozen, M. van der Burg, and K. Boztug. 2019. Polymerase δ deficiency causes syndromic immunodeficiency with replicative stress. *J Clin Invest*

25. Bellelli, R., V. Borel, C. Logan, J. Svendsen, D. E. Cox, E. Nye, K. Metcalfe, S. M. O'Connell, G. Stamp, H. R. Flynn, A. P. Snijders, F. Lassailly, A. Jackson, and S. J. Boulton. 2018. Polε Instability Drives Replication Stress, Abnormal Development, and Tumorigenesis. *Mol Cell* https://doi.org/10.1016/j.molcel.2018.04.008 :

bioRxiv preprint doi: https://doi.org/10.1101/2019.12.17.879544; this version posted December 18, 2019. The copyright holder for this preprint (which was not certified by peer review) is the author/funder, who has granted bioRxiv a license to display the preprint in perpetuity. It is made available under aCC-BY-NC-ND 4.0 International license.

26. Kokoska, R. J., L. Stefanovic, J. DeMai, and T. D. Petes. 2000. Increased rates of genomic deletions generated by mutations in the yeast gene encoding DNA polymerase delta or by decreases in the cellular levels of DNA polymerase delta. *Mol Cell Biol* 20: 7490-7504.

27. Zheng, D. Q., K. Zhang, X. C. Wu, P. A. Mieczkowski, and T. D. Petes. 2016. Global analysis of genomic instability caused by DNA replication stress in Saccharomyces cerevisiae. *Proc Natl Acad Sci U S A* 113: E8114-E8121.

28. Zheng, D. Q., and T. D. Petes. 2018. Genome Instability Induced by Low Levels of Replicative DNA Polymerases in Yeast. *Genes (Basel)* 9:

29. Prindle, M. J., and L. A. Loeb. 2012. DNA polymerase delta in DNA replication and genome maintenance. *Environ Mol Mutagen* 53: 666-682.

30. Burgers, P. M., and K. J. Gerik. 1998. Structure and processivity of two forms of Saccharomyces cerevisiae DNA polymerase delta. *J Biol Chem* 273: 19756-19762.

31. Acharya, N., R. Klassen, R. E. Johnson, L. Prakash, and S. Prakash. 2011. PCNA binding domains in all three subunits of yeast DNA polymerase {delta} modulate its function in DNA replication. *Proc Natl Acad Sci U S A*

32. Johnson, R. E., L. Prakash, and S. Prakash. 2012. Pol31 and Pol32 subunits of yeast DNA polymerase delta are also essential subunits of DNA polymerase zeta. *Proc Natl Acad Sci U S A*

33. Nishimura, K., T. Fukagawa, H. Takisawa, T. Kakimoto, and M. Kanemaki. 2009. An auxin-based degron system for the rapid depletion of proteins in nonplant cells. *Nat Methods* 6: 917-922.

34. Pardo, B., L. Crabbé, and P. Pasero. 2017. Signaling pathways of replication stress in yeast. *FEMS Yeast Res* 17:

35. Haruki, H., J. Nishikawa, and U. K. Laemmli. 2008. The anchor-away technique: rapid, conditional establishment of yeast mutant phenotypes. *Mol Cell* 31: 925-932.

36. McGuffee, S. R., D. J. Smith, and I. Whitehouse. 2013. Quantitative, Genome-Wide Analysis of Eukaryotic Replication Initiation and Termination. *Mol Cell* 50: 123-135.

bioRxiv preprint doi: https://doi.org/10.1101/2019.12.17.879544; this version posted December 18, 2019. The copyright holder for this preprint (which was not certified by peer review) is the author/funder, who has granted bioRxiv a license to display the preprint in perpetuity. It is made available under aCC-BY-NC-ND 4.0 International license.

37. Raghuraman, M. K., E. A. Winzeler, D. Collingwood, S. Hunt, L. Wodicka, A. Conway, D. J. Lockhart, R. W. Davis, B. J. Brewer, and W. L. Fangman. 2001. Replication dynamics of the yeast genome. *Science* 294: 115-121.

38. Kahli, M., J. S. Osmundson, R. Yeung, and D. J. Smith. 2018. Processing of eukaryotic Okazaki fragments by redundant nucleases can be uncoupled from ongoing DNA replication in vivo. *Nucleic Acids Res*

39. Ganai, R. A., X. P. Zhang, W. D. Heyer, and E. Johansson. 2016. Strand displacement synthesis by yeast DNA polymerase ε. *Nucleic Acids Res* 44: 8229-8240.

40. Mossi, R., R. C. Keller, E. Ferrari, and U. Hübscher. 2000. DNA polymerase switching: II. Replication factor C abrogates primer synthesis by DNA polymerase alpha at a critical length. *J Mol Biol* 295: 803-814.

41. Kreisel, K., M. K. M. Engqvist, J. Kalm, L. J. Thompson, M. Boström, C. Navarrete, J. P. McDonald, E. Larsson, R. Woodgate, and A. R. Clausen. 2019. DNA polymerase η contributes to genome-wide lagging strand synthesis. *Nucleic Acids Res* 47: 2425-2435.

42. Nick McElhinny, S. A., D. Kumar, A. B. Clark, D. L. Watt, B. E. Watts, E. B. Lundstrom, E. Johansson, A. Chabes, and T. A. Kunkel. 2010. Genome instability due to ribonucleotide incorporation into DNA. *Nat Chem Biol* 6: 774-781.

43. Wang, M., C. J. Herrmann, M. Simonovic, D. Szklarczyk, and C. von Mering. 2015. Version 4.0 of PaxDb: Protein abundance data, integrated across model organisms, tissues, and cell-lines. *Proteomics* 15: 3163-3168.

44. Lewis, J. S., L. M. Spenkelink, G. D. Schauer, O. Yurieva, S. H. Mueller, V. Natarajan, G. Kaur, C. Maher, C. Kay, M. E. O'Donnell, and A. M. van Oijen. 2019. Tunability of DNA Polymerase Stability during Eukaryotic DNA Replication. *Mol Cell*

45. Kapadia, N., Z. W. El-Hajj, T. R. Beattie, A. Yu, and R. Reyes-Lamothe. 2019. Processive activity of the replicative DNA polymerases in the replisome of live eukaryotic cells.

bioRxiv preprint doi: https://doi.org/10.1101/2019.12.17.879544; this version posted December 18, 2019. The copyright holder for this preprint (which was not certified by peer review) is the author/funder, who has granted bioRxiv a license to display the preprint in perpetuity. It is made available under aCC-BY-NC-ND 4.0 International license.

46. Kitamura, E., J. J. Blow, and T. U. Tanaka. 2006. Live-cell imaging reveals replication of individual replicons in eukaryotic replication factories. *Cell* 125: 1297-1308.

47. Yuan, Z., R. Georgescu, R. L. A. Santos, D. Zhang, L. Bai, N. Y. Yao, G. Zhao, M. E. O'Donnell, and H. Li. 2019. Ctf4 organizes sister replisomes and Pol α into a replication factory. *Elife* 8:

48. Reagan, M. S., C. Pittenger, W. Siede, and E. C. Friedberg. 1995. Characterization of a mutant strain to Saccharomyces Cerevisiae with a deletion of the RAD27 gene, a structural homolog of the RAD2 nucleotide excision-repair gene. *J Bacteriol* 177: 364-371.

49. Tishkoff, D. X., A. L. Boerger, P. Bertrand, N. Filosi, G. M. Gaida, M. F. Kane, and R. D. Kolodner. 1997. Identification and characterization of Saccharomyces cerevisiae EXO1, a gene encoding an exonuclease that interacts with MSH2. *Proc Natl Acad Sci U S A* 94: 7487-7492.

50. Spies, J., C. Lukas, K. Somyajit, M. B. Rask, J. Lukas, and K. J. Neelsen. 2019. 53BP1 nuclear bodies enforce replication timing at under-replicated DNA to limit heritable DNA damage. *Nat Cell Biol*

51. Morawska, M., and H. D. Ulrich. 2013. An expanded tool kit for the auxin-inducible degron system in budding yeast. *Yeast* 30: 341-351.

52. Smith, D. J., T. Yadav, and I. Whitehouse. 2015. Detection and Sequencing of Okazaki Fragments in S. cerevisiae. *Methods Mol Biol* 1300: 141-153.

53. Orebaugh, C. D., S. A. Lujan, A. B. Burkholder, A. R. Clausen, and T. A. Kunkel. 2018. Mapping Ribonucleotides Incorporated into DNA by Hydrolytic End-Sequencing. *Methods Mol Biol* 1672: 329-345.

54. Jiang, C., and B. F. Pugh. 2009. A compiled and systematic reference map of nucleosome positions across the Saccharomyces cerevisiae genome. *Genome Biol* 10: R109.

55. MacIsaac, K. D., T. Wang, D. B. Gordon, D. K. Gifford, G. D. Stormo, and E. Fraenkel. 2006. An improved map of conserved regulatory sites for Saccharomyces cerevisiae. *BMC Bioinformatics* 7: 113.